Applied Mathematical Modelling 132 (2024) 252–273

Contents lists available at ScienceDirect

Applied Mathematical Modelling

journal homepage: www.elsevier.com/locate/apm

A semi-analytical time-domain model with explicit fluid force expressions for fluidelastic vibration of a tube array in crossflow

Pan Sun [a,1], Xielin Zhao [a,1], Fengchun Cai [b], Huanhuan Qi [b], Jian Liu [b], Zhipeng Feng [b], Jinxiong Zhou [a,*]

[a] State Key Laboratory for Strength and Vibration of Mechanical Structures and School of Aerospace, Xi'an Jiaotong University, Xi'an 710049, People's Republic of China

[b] Key Laboratory of Nuclear Reactor System Design Technology, Nuclear Power Institute of China, Chengdu 610200, People's Republic of China

ARTICLE INFO

Keywords:
Fluidelastic instability
Semi-analytical time-domain model
Frequency-domain model
Bifurcation
Chaos

ABSTRACT

It is widely acknowledged that fluidelastic instability (FEI), among other mechanisms, is of the greatest concern in the flow-induced vibration (FIV) of tube bundles in steam generators and heat exchangers. A range of theoretical models have been developed for FEI analysis, and, in addition to the earliest semi-empirical Connors' model, the unsteady model, the quasi-steady model and the semi-analytical model are believed to be three advanced models predominant in the literature. The unsteady and the quasi-static models share the merits of having explicit fluid force expressions and ease of being implemented but require more experimental inputs, whereas the semi-analytical model requires fewer parameters due to its analytical nature but is hard, if not prohibitive, to derive explicit fluid force expressions. Since the fluid force formulations set in the core of development of FEI models, the understanding and in particular the implementation of the semi-analytical model has been impaired by the nonexistence of explicit fluid force expression. This issue becomes more profound in time-domain analysis whereby the simple harmonic assumption is discarded. Here we report a new semi-analytical time-domain (SATD) FEI model with explicit fluid force expressions. The new model allows a consistent frequency-domain stability analysis and more importantly a truly time-domain response analysis. The theory was validated by calculating linear stability thresholds of two typical tube array patterns and comparing against reported experimental data. We then present a nonlinear time-domain analysis of a single loosely-supported tube with piece-wise linear stiffness. The nonlinear and nonsmooth dynamics was probed in details by utilizing various techniques, playing an emphasis on characterizing and distinguishing the chaotic vibration. We found that the system follows a quasi-periodic route to chaos. Such an in-depth study of the nonlinear dynamics of tubes in crossflow has never been reported in the context of SATD model. Our results enrich the theory and provide a different approach for linear and nonlinear dynamics of tube bundles, which are essential for the subsequent fretting wear analysis.

* Corresponding author.
E-mail address: jxzhouxx@mail.xjtu.edu.cn (J. Zhou).
[1] Equal contribution.

https://doi.org/10.1016/j.apm.2024.04.044
Received 3 May 2023; Received in revised form 9 October 2023; Accepted 18 April 2024

Available online 29 April 2024

1. Introduction

The elegant model of cylindrical tubes or rods subjected to axial or crossflow represents the flow-induced vibrations (FIV) of a wide range of components and structures, like steam generators, heat exchangers, fluid-conveying pipes and transmission lines. In particular, FIV has long been considered as an integral part of design of nuclear plant in the same sense as reactor physics and thermohydraulics [1]. Excessive FIV would cause fatigue cracks and fretting wear damage of components, constituting a particular concern for stream generators and nuclear fuels. Considerable progress has been achieved in the past decades. The review papers by Blevins [2], Paidoussis [1,3], Pettigrew et al. [4,5], Weaver and Fitzpatrick [6], and Price [7], as well as monographs by Chen [8], Paidoussis [9,10], Au-Yang [11–13] provide excellent reviews on this field. Great efforts have been dedicated to FIV problems, and the main mechanisms of FIV have been elucidated to include turbulent buffetting, vortex shedding, fluidelastic instability (FEI) and acoustic resonance. FEI, among these mechanisms, is of the greatest concern for destructive damage of steam generators and heat exchangers.

Because of its destructive nature of FEI, extensive researches, both experimental and theoretical, have been carried out, aiming at understanding mechanism of FEI and deriving guidelines for engineering design. Despite some progress, the underlying mechanism of FEI remains puzzling due to the complicated nature of the problem, and it remains a sought-after task to develop FEI models to interpret experiment phenomena, and more importantly, to perform predictive designs and diagnosing analyses. A range of FEI models have been developed over the last 50 years to predict FEI thresholds and the associated post-instability responses, focusing largely on crossflow, single and two-phase flow. Having an appropriate FEI model, one can perform FEI analysis of a tube bundle given flow conditions, tube array pattern, mass and structural parameters of the tubes, etc. The FEI analysis can be either frequency-domain stability analysis or time-domain dynamic response analysis, or both. The difference between these two types of analysis can be understood as follows. A frequency-domain analysis is essentially a linear perturbation analysis, thus it adopts the harmonic solution assumption and it determines the stability threshold. Frequency-domain analysis is performed in the frequency domain, and the stability conditions are attained by performing an eigenvalue analysis of the FIV system and then evaluating the sign of the real part of the complex frequency. Time-domain analysis aims to obtain the time history of the vibration system, which is crucial for fatigue life prediction and fretting wear evaluation. Of course, by observing the convergent or divergent property of the time-history, the critical conditions for the onset of FEI can also be attained readily through a time-domain analysis. In this sense, time-domain analysis is more generic than frequency-domain analysis. Moreover, the frequency-domain analysis is a linear stability analysis and valid only for linear systems, whereas time-domain analysis works for either linear or nonlinear systems.

In the early stage of study on the FEI of tube bundles, attention was paid to prevention design and several semi-empirical models were developed exclusively for frequency-domain analysis, and these models are sometimes called frequency-domain FEI models. These frequency-domain models include the Jet-switch model by Roberts [14], the quasi-static model by Connors and by Blevins [15–17]. These semi-empirical models, such as the well-known Connors' equation, $\frac{U_c}{f_n D} = K\left(\frac{m\delta}{\rho D^2}\right)^{0.5}$, gives an analytical expression on critical reduced velocity, $\frac{U_c}{f_n D}$, against mass-damping-parameter (MDP), $\frac{m\delta}{\rho D^2}$, where f_n is the tube natural frequency, D is the tube diameter, m is the tube mass per unit length, δ is the logarithmic decrement of damping, ρ is the fluid density, K is a constant determined from experiment. The Connors' equation was widely used in engineering practice due to its simplicity and has achieved some success. Nevertheless, the Connors' formula was originally derived for a single row of cylinders, and its extension to tube arrays as well as the choice of reasonable value of Connors constant K causes controversy. Very recently, Shinde et al. [18] proposed a new theoretical model and applied it for FEI analysis of normal-square and other tube arrays, and good agreement was achieved. The model looks similar to the Connors' equation, but it incorporates the contribution of mechanical impedance with the constant of proportionality being expressed as a function of Euler number. To overcome the deficiency of quasi-static models, several quasi-steady or unsteady models have been proposed. These include the unsteady FEI model by Tanka and Takahara [19,20], and the unsteady model by Chen [8,21–23], the quasi-steady model by Price and Paidoussis [24,25] and the semi-analytical model by Lever and Weaver [26–28] and Yetisir and Weaver [29–32]. Although the unsteady model seems to be the most complete in theory, it is, in practice, difficult to use because there are extensive unsteady fluid force coefficients required to be determined through experiment. The semi-analytical model was derived analytically from the first principles of unsteady flow mechanics, and thus uses fewer experimental inputs as compared to the unsteady model and the quasi-steady model. The quasi-steady model can be regarded as a compromise between the unsteady model and the semi-analytical model. The unsteady and the quasi-steady model are coefficient-based models with explicit expression of fluid force, whereas it is not available in the semi-analytical model to date. In addition, the theory of the quasi-steady model and the semi-analytical model also accounts for the importance of time delay or phase lag in FEI. As mentioned, in the early stage of FEI study, all these models were used for frequency-domain analysis.

The frequency-domain analysis discussed above can only be used to predict the threshold of FEI. Investigators have been interested in post-instability dynamics of tube arrays, which is crucial for fatigue analysis and fretting-wear simulation. In steam generators or heat exchangers, the tubes are loosely supported by tube support plates (TSP) or sometimes constrained by anti-vibration bars (AVB). The clearance between the tube and the support as well as the one-sided vibration constraint gives rise to structural nonlinearity coupled to fluid-structure interaction. This makes the problem more challenging, and necessitates the need for performing nonlinear time-domain analysis. Fricker [33] derived a destabilizing fluid force expression based on the Connors' quasi-static model and employed the fluid force to model the dynamics of a tube loosely supported by an AVB. Fricker also implemented the fluid force into the finite element method (FEM) to model nonlinear dynamics of U-tubes in steam generators [34]. Eisinger et al. [35] incorporated frequency-dependent fluid forces derived from the unsteady FEI model by Chen into ABAQUS, and simulated the dynamic response of a U-tube with clearance at supports. Sawadogo and Mureithi [36,37] implemented the fluid force equation using the quasi-steady

model into a user subroutine UEL in ABAQUS for two-phase crossflow. Piteau et al. [38] investigated the vibro-impact responses of loosely-supported tubes subjected to turbulence force and fluid force using the unsteady model of Tanaka and Takahara [20]. All the above-Mentioned time-domain analyses stick to a fundamental assumption that the vibration is simply harmonic, thus giving a frequency-dependent fluid force. The single harmonic assumption also dramatically simplifies the incorporation of time-delay or phase lag. The two merits of harmonic approximation make the FEI analysis achievable. The harmonic solution assumption, however, is rigorously accurate only in the vicinity of the critical velocity, whereby the solution is nearly harmonic containing only one harmonic. For velocity away from the critical velocity, the single harmonic approximation is no longer valid, though the solution may still be periodic. Furthermore, the biggest deficiency of the use of frequency-dependent fluidelastic lies in the fact that the instantaneous vibration frequency can not be determined a priori, and this causes delicate problems in implementations.

It is highly desirable to perform truly time-domain FEI analysis for arbitrary tube motion. Paidoussis and Li [39] conducted the pioneer work towards this direction using the quasi-steady model and coefficient-based fluid force expressions. They presented a time-domain analysis of the response of a loosely-supported tube within an in-line array. Limit cycles, bifurcation as well as chaotic motion were captured by using the quasi-steady FEI model. Mureithi et al. [40,41] also employed the quasi-steady model to investigate the post-Hopf bifurcation response of a loosely-supported cylinder in a tube array. Two mechanisms leading to chaos were identified: A switching mechanism and the intermittency route. Good agreement was achieved between theoretical prediction and experimental observation. Very recently, we propose to use the incremental harmonic balance (IHB) method to calculate the periodic solution of nonlinear vibration of steam generator tubes based on the quasi-steady model [42]. A numerical strategy for multi-harmonic IHB analysis of high-dimensional delay differential equations (DDEs) as well combination of IHB with FEM are demonstrated. In a series of papers, Hassan and his co-workers extended the original semi-analytical by Lever and Weaver and presented a truly time-domain model. In the model, no assumption was made regarding the tube response, and instead the response was computed using a step-by-step time integration [43–47]. Anderson et al. [48] extended the time-domain model to analyze FEI of a square in-line tube array including the temporal variations in the flow separation. The SATD FEI model proposed by Hassan et al. provides an attractive numerical tool for truly time-domain nonlinear response analysis. The dynamic tube/support impact and sliding force as well as the wear rate captured by the model provide useful guidance for the predictive design and wear life evaluation of steam generators. Due to its analytical nature, and in particular the feature that requires the fewest experimental parameters, the development of SATD FEI model has spurred increasing interests in the field of FIV. Unfortunately, the fluid forces deduced from the semi-analytical models by Hassan et al. do not posses the merits of that derived from the unsteady model and the quasi-static model in which fluid forces are given as explicit functions of displacement, velocity and acceleration. The fluid force in the Hassan's model is given in a black-box integral form. If the integral form of fluid force is expanded into separate terms, there are single, double and triple integrals with fixed or variable limits. The implementation of the SATD model has been impaired by the nonexistence of explicit fluid force expressions and by the multiple integrals. No efforts have been made to derive an explicit formulation of fluid force in the context of SATD for arbitrary time-dependent vibrations. Here we report our new formulation for SATD FEI analysis. Our theory analytically derives the explicit fluid force expressions for very the first time. The closed-form fluid force includes coefficient-like stiffness, damping and mass terms, as well as multiple integrals having field variables at previous instants. The latter was computed numerically by using the stored previous response history and by a conventional Gaussian quadrature.

The biggest beauty of the current model is that the explicit coefficient terms associated with current response can be combined into structural mass, damping and stiffness terms, while the integral terms associated with time delays are treated as a load vector and assembled into the general load vector the same as the impact force. We demonstrate how this eases the implementation of Galerkin discretization of a vibrating beam. This is actually the core of FEM or mode truncation. We present a benchmark problem by approximating the tube as a single-degree-of-freedom (SDOF) oscillator or a continuous beam. As a special case, we also describe a frequency-domain stability analysis by assuming a harmonic solution. The linear stability analysis coincides with the truly time-domain analysis and agrees well with available experimental data.

The extension of the current model into nonlinear vibration problems is straightforward. Detailed nonlinear dynamic analyses are essential for the prevention design and diagnosis analysis of flow-induced vibration (FIV) of loosely supported tubes in steam generators and heat exchangers [40,41,49,50]. Nonlinear post-instability behavior of a tube array has been examined in the context of the unsteady model by Cai and Chen [51], and in the context of the quasi-steady model by Paidoussis and Li [52], Lai et al. [53]. and by Mureithi et al. [40,41], respectively. Fruitful nonlinear phenomena were successively captured by these two FEI models, and in-depth nonlinear analyses were reported, including bifurcations and chaos. In the context of the semi-analytical model, however, only simple response history of loosely supported tubes was reported by Hassan et al. [43–46]. Compared with the unsteady and the quasi-steady models, the semi-analytical model requires fewer experimental inputs and has gained increasing attention due to its analytical feature. There is a void to explore nonlinear dynamics of a tube array with loose support using the semi-analytical model. Here, we probe in details the nonlinear dynamics of loosely supported tubes in crossflow. Loose support can be approximated either by a cubic spring or by a discontinuous piece-wise linear model. The former is smooth while the latter is non-smooth and is more challenging. We report nonlinear dynamics of FIV of a cylinder with piece-wise linear spring. The results have not yet been reported elsewhere, which open a door for studying nonlinear dynamics of loosely supported tubes in a variety of power plant equipment and components. These detailed dynamic responses are crucial for fatigue analysis and in particular for fretting wear analysis.

The paper is organized as follows. The SATD model is reformulated in Section 2, adopting the identical assumptions used by Lever and Weaver, but discarding the harmonic solution assumption. Explicit forms of fluid forces are derived in Section 2.2. For a vibrating beam, the spatial discretization using Galerkin mode truncation is given in Section 2.3. Based on the proposed SATD FEI model, a stability analysis is carried out readily in Section 2.4 by adopting again the harmonic solution. The frequency-domain and

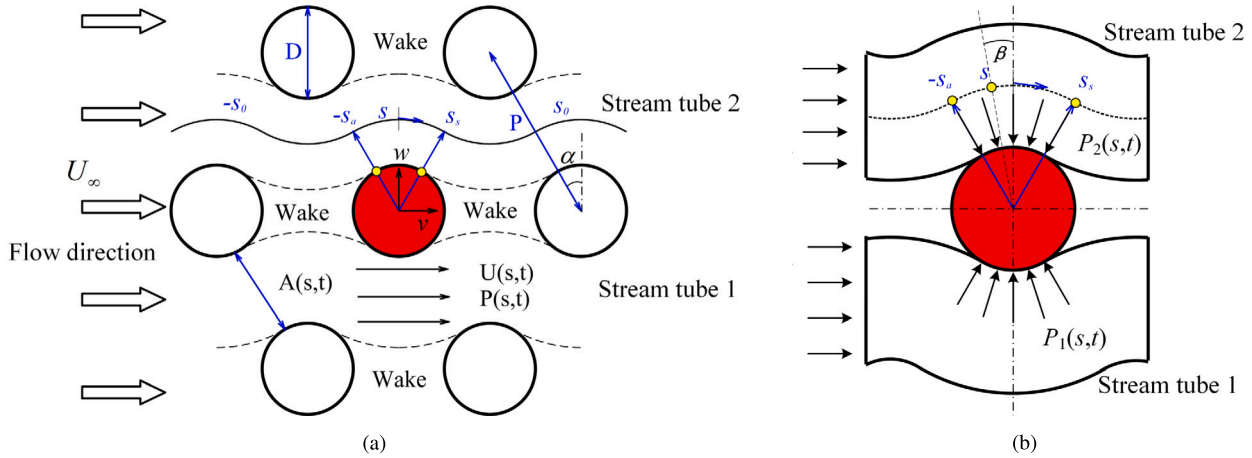

Fig. 1. A schematic of the problem considered where an elastic tube (marked in red) is vibrating in an otherwise rigid parallel triangle tube array subjected to crossflow. (a) The ingredients of the SATD model for FEI of a tube array are illustrated here. (b) The schematic of the pressure distribution around the flexible tube.

the linear time-domain analysis results are presented in Section 3. Nonlinear dynamics of a loosely-supported tube in a tube rigid tube array is explored and presented in Section 4, and finally some concluding remarks follow in Section 5.

2. New formulations for SATD FEI model

2.1. Classical SATD model

Without loss of generality, the parallel triangle tube array is chosen as an example and shown schematically in Fig. 1. For the purpose of simplicity and making the story short, only the FEI in the lift direction is considered here, but the theory described herein can be extended readily to model FEI in both transverse and streamwise directions. We here only consider the case that a single flexible, marked in red here, is surrounded by an otherwise rigid tube array. We only consider the case where the tube array is subjected to single-phase external flow. Fig. 1 illustrates the ingredients of the SATD model. The channels above and below and the central tube line are the so-called stream tubes. A curvilinear coordinate s in Fig. 1 (a) is used to describe the flow path along the stream tube. A coordinate $-s_0$ is used to designate the flow inlet far away from the flexible tube. The flexible tube in the middle is in contact with the stream tube at $-s_a \le s \le s_s$, where $-s_a$ and s_s are the flow attachment and separation positions, respectively. The flow attachment and separation positions and angles are either measured by experiments or by CFD simulations [54]. The parameters used in this paper is summarized and given in Appendix A. The average area of the stream tube is a constant and is taken as its minimum gap area A_0. In Fig. 1 (a), D is the tube diameter, P is the pitch of two adjacent tubes, and $P_r = P/D$ is the pith ratio.

When the flexible tube vibrates, the vibration generates perturbation to the stream tubes. The instantaneous stream tube area, $A(s,t)$, of the upper and lower stream tubes can be expressed in terms of the mean component, A_0, and the fluctuating component, $a(s,t)$, as follows,

$$A(s,t) = A_0 \pm a(s,t) \tag{1}$$

The area perturbation due to the vibration of the flexible tube is gradually dissipated from the attachment position s_a to the inlet s_0, and this is reflected by a decay function $\gamma(s)$. At large distance from the flexible tube, the disturbance is negligible and thus $\gamma(s) = 0$ as $s \to \infty$. Also a time delay function $\tau(s)$ should be introduced to account for the after-effect phenomenon. Thus the area perturbation at any point, $a(s,t)$, is related to tube vibration displacement w as

$$a(s,t) = w[t\text{-}\tau(s)]\gamma(s) \tag{2}$$

There are several forms of possible decay and time delay functions, and we adopt the following popular ones in this paper:

$$\tau(s) = \begin{cases} -\dfrac{\varepsilon s_0}{U_0}\dfrac{s+s_a}{s_0-s_a} & -s_0 < s < -s_a \\ 0 & -s_a \le s \le s_s \\ -\dfrac{\varepsilon s_0}{U_0}\dfrac{s_s-s}{s_0-s_s} & s_s < s < s_0 \end{cases} \tag{3}$$

and

$$\gamma(s)=\begin{cases}\dfrac{s+s_0}{s_0-s_a} & -s_0<s<-s_a\\ 1.0 & -s_a\le s\le s_s\\ \dfrac{s_0-s}{s_0-s_s} & s_s<s<s_0\end{cases} \tag{4}$$

Though various forms of decay functions and time delay functions used in literatures vary in form, they almost all reflect an experimental fact that, along the tube contact region, $-s_a \le s \le s_s$, there is no area perturbation decay and no time delay and thus $\gamma(s)=1.0$ and $\tau(s)=0$. Following the same way as area perturbation, the fluctuations of flow velocity and pressure due to vibration of the tube can be expressed using the average value (U_0, P_0) and the perturbation components $(u(s,t), p(s,t))$ as follows,

$$U(s,t)=U_0+u(s,t) \tag{5}$$

and

$$P(s,t)=P_0+p(s,t) \tag{6}$$

The mean flow velocity of stream tube U_0 in Eq. (5) can be obtained from the following relation,

$$U_0=\frac{U_r f_n D(P-D)\cos\alpha}{A_0} \tag{7}$$

where $f_n=\omega_n/(2\pi)$ is the tube natural frequency, α is the tube array geometry angle defined in Fig. 1(a), and U_r is the reduced velocity.

Considering the control body consisting of a segment of the stream tube, the continuity equation along the coordinate s can be written as

$$\frac{\partial A(s,t)}{\partial t}+\frac{\partial A(s,t)U(s,t)}{\partial s}=0 \tag{8}$$

Substituting Eq. (1) and Eq. (5) into Eq. (8) and integrating over the coordinate s, the velocity fluctuations of lower stream tube, denoted by stream tube 1, and that of the upper stream tube, marked by stream tube 2, can be calculated as

$$u_1(s,t)=\frac{1}{A_0+a(s,t)}\left[-U_0 a(s,t)-\int_{-s_0}^{s}\dot{a}(s,t)\,ds\right] \tag{9}$$

and

$$u_2(s,t)=\frac{1}{A_0\text{-}a(s,t)}\left[U_0 a(s,t)+\int_{-s_0}^{s}\dot{a}(s,t)\,ds\right] \tag{10}$$

A subtraction between $u_2(s,t)$ and $u_1(s,t)$ and discard of high-order terms gives

$$u_2(s,t)-u_1(s,t)=\frac{2}{A_0}\left[U_0 a(s,t)+\int_{-s_0}^{s}\dot{a}(s,t)\,ds\right] \tag{11}$$

The momentum equation of the system can be described by the one-dimensional unsteady Bernoulli equation as

$$\frac{1}{\rho}\frac{\partial P(s,t)}{\partial s}+U(s,t)\frac{\partial U(s,t)}{\partial s}+\frac{\partial U(s,t)}{\partial t}+\frac{h}{2s_0}U(s,t)^2=0 \tag{12}$$

where the last term in Eq. (12) accounting for the turbulent losses of the mean flow around the flexible tube and being expressed as a drag force proportional to the square of the local velocity with h being the flow resistance coefficient. The experimental loss coefficient h of Pierson [55] which determined by tube array configuration have been used here. Performing integration of Eq. (12) from $-s_0$ to s gives the following relation,

$$\frac{1}{\rho}\left[P(s,t)-P(-s_0,t)\right]+\frac{1}{2}\left[U^2(s,t)-U^2(-s_0,t)\right]+\int_{-s_0}^{s}\frac{\partial U(s,t)}{\partial t}ds+\frac{h}{2s_0}\int_{-s_0}^{s}U^2(s,t)ds=0 \tag{13}$$

Plugging Eq. (6) into Eq. (13) and invoking $P(-s_0,t)=P_0$ and $U(-s_0,t)=U_0$ gives the pressure fluctuation as

$$p(s,t)=\rho\left[\frac{1}{2}U_0{}^2-\frac{1}{2}U^2(s,t)-\int_{-s_0}^{s}\frac{\partial U(s,t)}{\partial t}ds-\frac{h}{2s_0}\int_{-s_0}^{s}U^2(s,t)ds\right] \tag{14}$$

Substituting Eq. (14) and Eq. (5) into Eq. (6), the pressures in stream tube 1 and 2 thus being derived respectively as

$$P_1 = P_0 + \rho\left[-U_0 u_1(s,t) - \int_{-s_0}^{s} \frac{\partial u_1(s,t)}{\partial t} ds_1 - \frac{h}{2s_0}\int_{-s_0}^{s} \left(U_0{}^2 + 2U_0 u_1(s,t)\right) ds_1\right] \tag{15}$$

$$P_2 = P_0 + \rho\left[-U_0 u_2(s,t) - \int_{-s_0}^{s} \frac{\partial u_2(s,t)}{\partial t} ds_1 - \frac{h}{2s_0}\int_{-s_0}^{s} \left(U_0{}^2 + 2U_0 u_2(s,t)\right) ds_1\right] \tag{16}$$

With Eq. (15) and Eq. (16) in hand, the lift force per unit length on a flexible tube can be given as

$$F_L = \int_{-s_a}^{s_s} \left[P_1(s,t) - P_2(s,t)\right] \cos\beta(s) ds \tag{17}$$

where $\beta = 2s/P$ is the angle made between the surface normal and the transverse axis of the tube. Eq. (17) is the black-box fluid force expression used by Hassan et al. [43–47] for time-domain FEI analysis. The interplay between the lift force and the tube vibration is complex and obscure: The vibration of the flexible tube causes stream tube area perturbation, and stream tube area perturbation induces velocity and pressure fluctuations and eventually variation of lift force, which in turn induces vibration of the tube. This complex coupling reveals the physics and mechanism of this self-excited vibration.

2.2. New formulations for SATD model

The proceeding derivations from Eq. (1) to Eq. (17) are identical to classical SATD model. Our theory departs from the classical SATD model form the following derivations. Note that Eq. (17) can be rewritten as

$$F_L = \rho \int_{-s_a}^{s_s} \left\{ U_0\left(u_2 - u_1\right) + \int_{-s_0}^{s} \frac{\partial}{\partial t}\left(u_2 - u_1\right) ds_1 + \frac{hU_0}{s_0}\int_{-s_0}^{s} \left(u_2 - u_1\right) ds_1 \right\} \cos\beta(s) ds \tag{18}$$

and plugging Eq. (11) into Eq. (18) yields:

$$\begin{aligned} F_L = \frac{2\rho}{A_0}\Bigg[& U_0^2 \int_{-s_a}^{s_s} a \cdot \cos\beta ds + 2U_0 \int_{-s_a}^{s_s} \cos\beta(s) \int_{-s_0}^{s} \dot{a} ds_1 ds + \int_{-s_a}^{s_s} \cos\beta(s) \int_{-s_0}^{s}\int_{-s_0}^{s_1} \ddot{a} ds_2 ds_1 ds \\ & + \frac{hU_0^2}{s_0}\int_{-s_a}^{s_s} \cos\beta(s) \int_{-s_0}^{s} a ds_1 ds + \frac{hU_0}{s_0}\int_{-s_a}^{s_s} \cos\beta(s) \int_{-s_0}^{s}\int_{-s_0}^{s_1} \dot{a} ds_2 ds_1 ds \Bigg] \end{aligned} \tag{19}$$

The explicit five-term fluid force expression in terms of a, $\dot{a}$, and $\ddot{a}$ presented in Eq. (19) has not been given elsewhere. From Eq. (3) and Eq. (4) we emphasize once again that there is no time delay and no area perturbation decay in the tube contact region, thus Eq. (2) is rewritten as follows by using the piecewise definitions in Eq. (3) and Eq. (4)

$$a(s,t) = \begin{cases} w[t-\tau(s)]\gamma(s) & -s_0 < s < -s_a \\ w(t) & -s_a \le s \le s_s \\ w[t-\tau(s)]\gamma(s) & s_s < s < s_0 \end{cases} \tag{20}$$

The piecewise property presented in Eq. (20) can be utilized to perform integration by parts, separating terms associated with current vibration response from those with time delay. This is the crucial step in our new formulations. The details of the derivations can be found in Appendix B. Eq. (19) thus can be formulated as the following explicit coefficient-based form

$$\begin{aligned} F_L = {} & m_{FE}\ddot{w}(t) + c_{FE}\dot{w}(t) + k_{FE}w(t) \\ & + \int_{-s_a}^{s_s} \cos\beta(s) \int_{-s_0}^{-s_a} \left\{\alpha_1 \dot{w}[t\text{-}\tau(s_1)] + \alpha_3 w[t\text{-}\tau(s_1)]\right\} \gamma(s_1) ds_1 ds \\ & + \int_{-s_a}^{s_s} \cos\beta(s) \int_{-s_0}^{-s_a}\int_{-s_0}^{s_1} \left\{\alpha_2 \ddot{w}[t\text{-}\tau(s_2)] + \alpha_4 \dot{w}[t\text{-}\tau(s_2)]\right\} \gamma(s_2) ds_2 ds_1 ds \\ & + \int_{-s_a}^{s_s} \cos\beta(s) \int_{-s_a}^{s}\int_{-s_0}^{-s_a} \left\{\alpha_2 \ddot{w}[t\text{-}\tau(s_2)] + \alpha_4 \dot{w}[t\text{-}\tau(s_2)]\right\} \gamma(s_2) ds_2 ds_1 ds \end{aligned} \tag{21}$$

where s_1 and s_2 are two dummy integration variables. m_{FE}, c_{FE} and k_{FE} are the mass, damping and stiffness coefficients of the fluid force without time delay, and their explicit expressions are given as

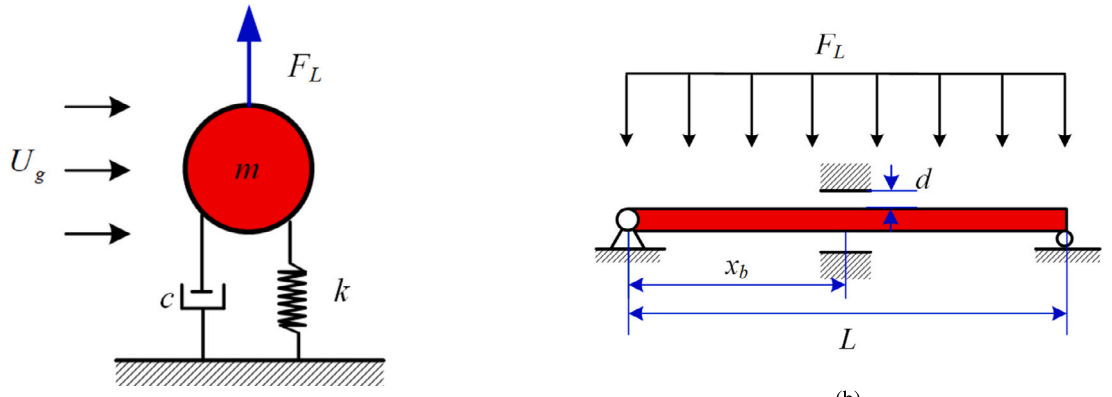

Fig. 2. The elastic tube in Fig. 1 can be either approximated by a SDOF spring-damper system (a) or a continuous beam loosely supported at distance x_b with clearance d (b).

$$m_{FE} = \frac{2\rho}{A_0}\int_{-s_a}^{s_s}\cos\beta(s)\int_{-s_a}^{s}\int_{-s_a}^{s_1} ds_2 ds_1 ds = \alpha_2\int_{-s_a}^{s_s}\cos\beta(s)\cdot\frac{(s+s_a)^2}{2}ds \tag{22}$$

$$\begin{aligned} c_{FE} &= \frac{4\rho U_0}{A_0}\int_{-s_a}^{s_s}\cos\beta(s)\int_{-s_a}^{s} ds_1 ds + \frac{2\rho h U_0}{A_0 s_0}\int_{-s_a}^{s_s}\cos\beta(s)\int_{-s_a}^{s}\int_{-s_a}^{s_1} ds_2 ds_1 ds \\ &= \int_{-s_a}^{s_s}\cos\beta(s)\cdot\left[\alpha_1(s+s_a) + \frac{\alpha_4(s+s_a)^2}{2}\right]ds \end{aligned} \tag{23}$$

$$\begin{aligned} k_{FE} &= \frac{2\rho {U_0}^2}{A_0}\int_{-s_a}^{s_s}\cos\beta(s)\,ds + \frac{2\rho h {U_0}^2}{A_0 s_0}\int_{-s_a}^{s_s}\cos\beta\int_{-s_a}^{s} ds_1 ds \\ &= \int_{-s_a}^{s_s}\cos\beta(s)\cdot\left[\alpha_5 + \alpha_3(s+s_a)\right]ds \end{aligned} \tag{24}$$

Where α_1, α_2, α_3, α_4 and α_5 are constants and defined as

$$\alpha_1 = \frac{4\rho U_0}{A_0},\quad \alpha_2 = \frac{2\rho}{A_0},\quad \alpha_3 = \frac{2\rho h {U_0}^2}{A_0 s_0},\quad \alpha_4 = \frac{2\rho h U_0}{A_0 s_0},\quad \alpha_5 = \frac{2\rho {U_0}^2}{A_0}$$

We believe in that, for very the first time, an explicit fluid force expression is derived in Eq. (21) in the framework of SATD model. Note that we adopt the same basic assumptions as the classical Lever and Weaver model, but the tube displacement can be arbitrary. All the formulations are derived from first-principles and no approximations are introduced in derivation of fluid force. However, we should admit that our formulations rely on a basic approximation that the fluid force of a single flexible tube in an otherwise rigid tube array could give a reasonable well approximation to that of a fully flexible tube array. This basic approximation was adopted intensively in the literature and was validated by many experiments. In addition, the time-delay function, Eq. (3), and the decay function, Eq. (4), are approximation to real stream tube morphology.

2.3. Time-domain FEI analysis based on SATD model

2.3.1. SATD model for SDOF system

The above-mentioned SATD model was firstly applied to an SDOF system schematically shown in Fig. 2 (a). The vibration equation for the time-domain analysis of such an SDOF system is given as

$$m\ddot{w} + c\dot{w} + kw = F_L \tag{25}$$

where m is the mass per unit length of the tube, $c = \delta m\omega_n/\pi$ is the damping coefficient and $k = m{\omega_n}^2$ is the stiffness coefficient. Substituting Eq. (21) into Eq. (25) and moving the mass, damping and stiffness coefficient terms to the left-hand gives

$$\left(m - m_{FE}\right)\ddot{w} + \left(c - c_{FE}\right)\dot{w} + \left(k - k_{FE}\right)w = F_{td} \tag{26}$$

where

$$F_{td} = \int_{-s_a}^{s_s} \cos\beta(s) \int_{-s_0}^{-s_a} \left\{\alpha_1 \dot{w}[t\text{-}\tau(s_1)] + \alpha_3 w[t\text{-}\tau(s_1)]\right\} \gamma(s_1) ds_1 ds + \int_{-s_a}^{s_s} \cos\beta(s) \int_{-s_0}^{-s_a} \int_{-s_0}^{s_1} \left\{\alpha_2 \ddot{w}[t\text{-}\tau(s_2)] + \alpha_4 \dot{w}[t\text{-}\tau(s_2)]\right\} \gamma(s_2) ds_2 ds_1 ds + \int_{-s_a}^{s_s} \cos\beta(s) \int_{-s_a}^{s} \int_{-s_0}^{-s_a} \left\{\alpha_2 \ddot{w}[t\text{-}\tau(s_2)] + \alpha_4 \dot{w}[t\text{-}\tau(s_2)]\right\} \gamma(s_2) ds_2 ds_1 ds$$

is the fluid force with time delay and can be evaluated numerically by using Gaussian quadrature. Eq. (26) is an SDOF differential equation with neutral delay and be solved by using a built-in function ddensd in MATLAB.

2.3.2. SATD model for a continuous beam

We then applied the SATD model to a continuous beam and the governing equation is given as

$$m\frac{\partial^2 w}{\partial t^2} + c\frac{\partial w}{\partial t} + EI\frac{\partial^4 w}{\partial x^4} = F_L \tag{27}$$

where w is the transverse displacement of the beam, EI is its flexural stiffness, and F_L is the fluid force given in Eq. (21). The following dimensionless quantities are introduced, where L denotes the tube length and λ_1 denotes the dimensionless eigenvalue of the first order mode of a simply supported beam.

$$\eta = \frac{w}{D}, \quad \xi = \frac{x}{L}, \quad \tilde{t} = \lambda_1^2\sqrt{\frac{EI}{mL^4}}t = \omega_n t, \quad \zeta = \frac{c}{m\omega_n}, \quad \tilde{m} = \frac{m}{\rho D^2},$$
$$\tilde{U}_0 = \frac{2\pi U_0}{D\omega_n}, \quad \tilde{s} = \frac{s}{D}, \quad \tilde{A}_0 = \frac{A_0}{D}, \quad \tilde{F}_L = \frac{F_L}{m{\omega_n}^2 D} \tag{28}$$

A dimensionless form of Eq. (27) is written as

$$\left(1 - \tilde{m}_{FE}\right)\frac{\partial^2 \eta}{\partial \tilde{t}^2} + \left(\zeta - \tilde{c}_{FE}\right)\frac{\partial \eta}{\partial \tilde{t}} + \frac{1}{{\lambda_1}^4}\frac{\partial^4 \eta}{\partial \xi^4} - \tilde{k}_{FE}\eta = \tilde{F}_{td}\left(\eta(\tilde{t}-\tilde{\tau}), \dot{\eta}(\tilde{t}-\tilde{\tau}), \ddot{\eta}(\tilde{t}-\tilde{\tau})\right) \tag{29}$$

in which F_{td} is the dimensionless form of the fluid force with time delay and other dimensionless coefficients are defined as

$$\tilde{m}_{FE} = \frac{m_{FE}}{m}, \quad \tilde{c}_{FE} = \frac{c_{FE}}{m\omega_n}, \quad \tilde{k}_{FE} = \frac{k_{FE}}{m\omega_n^2}$$
$$\tilde{\alpha}_1 = \alpha_1 \cdot \frac{D^2}{m\omega_n}, \quad \tilde{\alpha}_2 = \alpha_2 \cdot \frac{D^3}{m}, \quad \tilde{\alpha}_3 = \alpha_3 \cdot \frac{D^2}{m\omega_n^2}, \quad \tilde{\alpha}_4 = \alpha_4 \cdot \frac{D^3}{m\omega_n}, \quad \tilde{\alpha}_5 = \alpha_5 \cdot \frac{D}{m\omega_n^2}$$

Converting the PDE in Eq. (29) into a set of ODEs can be realized by using the mode truncation technique via a standard Galerkin procedure. The solution can be approximated as a mode summation as

$$\eta(\xi, \tilde{t}) = \sum_{j=1}^{M} N_j(\xi) q_j(\tilde{t}) \tag{30}$$

in which $q_j(\tilde{t})$ are the principle coordinates, M is the number of modes used for approximation, and $N_j(\xi)$ are vibration modes. Substituting Eq. (30) and performing the Galerkin procedure over Eq. (29) gives

$$\left(1 - \tilde{m}_{FE}\right)\ddot{q}_j(\tilde{t}) + \left(\frac{\delta v_j}{\pi} - \tilde{c}_{FE}\right)\dot{q}_j(\tilde{t}) + \left(v_j^2 - \tilde{k}_{FE}\right)q_j(\tilde{t}) = \tilde{F}_{td}\left(q_j(\tilde{t}-\tilde{\tau}), \dot{q}_j(\tilde{t}-\tilde{\tau}), \ddot{q}_j(\tilde{t}-\tilde{\tau})\right) \tag{31}$$

where $v_j = \left(\lambda_j/\lambda_1\right)^2$ is the ratio of the jth order to the first order dimensionless natural frequency of the beam. The spatial discretization scheme mentioned above is based on the linear vibration mode truncation, and other spatial discretization schemes can also be adopted and the procedure is identical. A time domain FEI analysis of a continuous beam is realized by solving the set of DDEs in Eq. (31).

2.4. Frequency-domain FEI analysis based on SATD model

The SATD model formulated above facilitates not only time-domain response analysis but also frequency-domain stability analysis. In sharp contrast to classical frequency-domain stability analysis, which assumes the simple harmonic solution at the very beginning of analysis and attains closed-form solution of velocity and pressure fluctuations only valid for limited forms of piecewise linear decay functions, the harmonic solution assumption is adopted to the final equation of motion, Eq. (25), and the formulation works

for whatever decay function. Now assume $w = w_0 \cdot e^{i\omega t}$, $\dot{w} = w_0 \cdot i\omega e^{i\omega t}$ and $\ddot{w} = -w_0 \cdot \omega^2 e^{i\omega t}$ with ω being the vibration complex frequency, $\omega = \omega_R + i \cdot \omega_I$, and note that $\omega_n = \sqrt{k/m}$ and $c = \delta m \omega_n / \pi$, Eq. (25) can be rewritten as

$$m \cdot \omega_n^2 \left[-\left(\frac{\omega}{\omega_n}\right)^2 + \frac{\delta}{\pi}\left(\frac{\omega}{\omega_n}\right) i + 1 \right] w_0 e^{i\omega t} = (F_R + i \cdot F_I) \cdot w_0 \cdot e^{i\omega t} \tag{32}$$

in which F_L is separated into real and imaginary parts and written as $F_L = (F_R + i \cdot F_I) \cdot w_0 \cdot e^{i\omega t}$. Introducing the following dimensionless quantities

$$\begin{aligned} &w^* = w/D, \qquad a^*(s,t) = a(s,t)/D, \qquad {A_0}^* = A_0/D, \qquad s^* = s/D, \\ &l_0^* = 2s_0^*, \qquad U_0^* = \frac{U_0}{\omega_n l_0} = \frac{U_0}{2\omega_n s_0}, \quad F_L^* = \frac{F_L}{\rho D^2 \omega_n^2} = F_R^* + i \cdot F_I^* \end{aligned} \tag{33}$$

Eq. (32) can be written as the following dimensionless form

$$\frac{m}{\rho D^2}\left[-\left(\frac{\omega}{\omega_n}\right)^2 + \frac{\delta}{\pi}\left(\frac{\omega}{\omega_n}\right) i + 1 \right] = F_R^* + i \cdot F_I^* \tag{34}$$

where

$$\begin{aligned} F_R^* = &-\left(\frac{\omega}{\omega_n}\right)^2 m_{FE}^* + k_{FE}^* + \int_{-s_a^*}^{s_s^*} \cos\beta\left(s^*\right) \int_{-s_0^*}^{-s_a^*} \{\alpha_3^* cos[\varphi\left(s_1^*\right)] + \alpha_1^*\left(\frac{\omega}{\omega_n}\right) sin[\varphi\left(s_1^*\right)]\}\gamma(s_1^*) ds_1^* ds^* \\ &+ \int_{-s_a^*}^{s_s^*} \cos\beta\left(s^*\right) \int_{-s_0^*}^{-s_a^*} \int_{-s_0^*}^{s_1^*} \{-\alpha_2^*\left(\frac{\omega}{\omega_n}\right)^2 cos[\varphi\left(s_2^*\right)] + \alpha_4^*\left(\frac{\omega}{\omega_n}\right) sin[\varphi\left(s_2^*\right)]\}\gamma(s_2^*) ds_2^* ds_1^* ds^* \\ &+ \int_{-s_a^*}^{s_s^*} \cos\beta\left(s^*\right) \int_{-s_a^*}^{s^*} \int_{-s_0^*}^{-s_a^*} \{-\alpha_2^*\left(\frac{\omega}{\omega_n}\right)^2 cos[\varphi\left(s_2^*\right)] + \alpha_4^*\left(\frac{\omega}{\omega_n}\right) sin[\varphi\left(s_2^*\right)]\}\gamma(s_2^*) ds_2^* ds_1^* ds^* \end{aligned} \tag{35}$$

and

$$\begin{aligned} F_I^* = &\left(\frac{\omega}{\omega_n}\right) c_{FE}^* + \int_{-s_a^*}^{s_s^*} \cos\beta\left(s^*\right) \int_{-s_0^*}^{-s_a^*} \{-\alpha_3^* sin[\varphi\left(s_1^*\right)] + \alpha_1^*\left(\frac{\omega}{\omega_n}\right) cos[\varphi\left(s_1^*\right)]\}\gamma(s_1^*) ds_1^* ds^* \\ &+ \int_{-s_a^*}^{s_s^*} \cos\beta\left(s^*\right) \int_{-s_0^*}^{-s_a^*} \int_{-s_0^*}^{s_1^*} \{-\alpha_2^*\left(\frac{\omega}{\omega_n}\right)^2 sin[\varphi\left(s_2^*\right)] + \alpha_4^*\left(\frac{\omega}{\omega_n}\right) cos[\varphi\left(s_2^*\right)]\}\gamma(s_2^*) ds_2^* ds_1^* ds^* \\ &+ \int_{-s_a^*}^{s_s^*} \cos\beta\left(s^*\right) \int_{-s_a^*}^{s^*} \int_{-s_0^*}^{-s_a^*} \{-\alpha_2^*\left(\frac{\omega}{\omega_n}\right)^2 sin[\varphi\left(s_2^*\right)] + \alpha_4^*\left(\frac{\omega}{\omega_n}\right) cos[\varphi\left(s_2^*\right)]\}\gamma(s_2^*) ds_2^* ds_1^* ds^* \end{aligned} \tag{36}$$

in which $\varphi(s^*) = \omega\tau(s^*)$ is the dimensionless phase lag function and $\gamma(s^*)$ is the dimensionless decay function, and are given as

$$\varphi(s^*) = \begin{cases} -\dfrac{\omega}{U_0^* \omega_n} \dfrac{s^* + s_a^*}{s_0^* - s_a^*} & -s_0^* < s^* < -s_a^* \\ 0 & -s_a^* \le s^* \le s_s^* \\ -\dfrac{\omega}{U_0^* \omega_n} \dfrac{s_s^* - s^*}{s_0^* - s_s^*} & s_s^* < s^* < s_0^* \end{cases}, \quad \gamma(s^*) = \begin{cases} \dfrac{s^* + s_0^*}{s_0^* - s_a^*} & -s_0^* < s^* < -s_a^* \\ 1.0 & -s_a^* \le s^* \le s_s^* \\ \dfrac{s_0^* - s^*}{s_0^* - s_s^*} & s_s^* < s^* < s_0^* \end{cases} \tag{37}$$

The dimensionless coefficients in Eq. (34) and (35) are given as follows

$$\begin{aligned} &m_{FE}^* = \frac{m_{FE}}{\rho D^2}, \qquad c_{FE}^* = \frac{c_{FE}}{\rho D^2 \omega_n}, \qquad k_{FE}^* = \frac{k_{FE}}{\rho D^2 \omega_n^2} \\ &\alpha_1^* = \alpha_1 \cdot \frac{1}{\rho \omega_n}, \quad \alpha_2^* = \alpha_2 \cdot \frac{D}{\rho}, \quad \alpha_3^* = \alpha_3 \cdot \frac{1}{\rho \omega_n^2}, \quad \alpha_4^* = \alpha_4 \cdot \frac{D}{\rho \omega_n}, \quad \alpha_5^* = \alpha_5 \cdot \frac{1}{\rho \omega_n^2 D} \end{aligned}$$

Multiplying both sides of Eq. (34) by $\left[1 - \left(\frac{\omega}{\omega_n}\right)^2 - \frac{\delta}{\pi}\left(\frac{\omega}{\omega_n}\right) i\right]$ gives

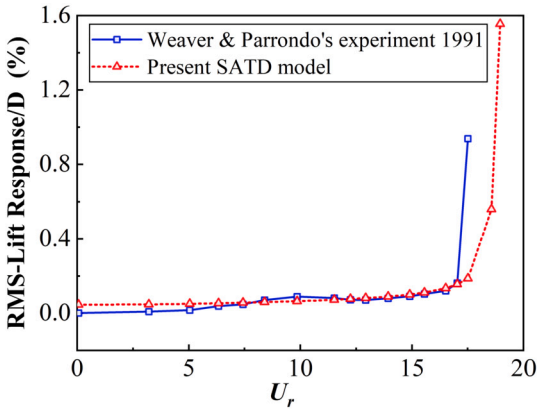

Fig. 3. Comparison of Weaver and Parrondo's experimental data for a parallel triangle array with pitch ratio 1.47 (blue line) and simulation of present SATD model (red dash line).

$$\frac{m}{\rho D^2}\left\{\left[1-\left(\frac{\omega}{\omega_n}\right)^2\right]^2+\left[\frac{\delta}{\pi}\left(\frac{\omega}{\omega_n}\right)\right]^2\right\}=F_R^*\left[1-\left(\frac{\omega}{\omega_n}\right)^2\right]+F_I^*\frac{\delta}{\pi}\left(\frac{\omega}{\omega_n}\right)+i\cdot F_I^*\left[1-\left(\frac{\omega}{\omega_n}\right)^2\right]-i\cdot F_R^*\frac{\delta}{\pi}\left(\frac{\omega}{\omega_n}\right) \tag{38}$$

The critical condition for the onset of FEI is dictated by $\omega_I=0$. Under this critical condition, the imaginary part of Eq. (38) vanishes, giving

$$\left(\frac{\omega}{\omega_n}\right)^2+\frac{\delta F_R^*}{\pi F_I^*}\left(\frac{\omega}{\omega_n}\right)-1=0 \tag{39}$$

Denoting

$$\frac{\omega}{\omega_n}=-\frac{b}{2}+\sqrt{\frac{b^2}{4}+1}, \quad b=\frac{\delta F_R^*}{\pi F_I^*} \tag{40}$$

we finally come up with the following stability conditions

$$\frac{\pi F_I^*}{\left(\frac{\omega}{\omega_n}\right)}=\frac{m\delta}{\rho D^2} \tag{41}$$

In Eq. (41), F_I^* is an implicit function of U_r, and Eq. (41) relates the critical reduced velocity to MDP of the tube. Eq. (41) is solved iteratively and the stability diagram is plotted as ${U_r}^c$ versus MDP.

3. Linear dynamics of a single flexible tube in crossflow

The vibration of the flexible tube in an otherwise rigid tube array in Fig. 1 can be approximated as vibration of an SDOF spring-damper vibrating system or vibration of a continuous beam, all subjected to crossflow-induced lift force. These two systems are shown schematically in Fig. 2 (a) and Fig. 2 (b), respectively. This paper is mainly focusing on results obtained from the SDOF system, and the results of vibrating beam are similar to those of SDOF system and would be briefly discussed.

The current SATD model was applied to two typical tube array configurations widely used in engineering practice: a parallel triangle tube array with pitch ratio 1.47 and MDP = 17.35, and an in-line square tube array with pitch ratio 1.5 and MDP = 60. A time-domain FEI analysis was performed and the vibration response was readily obtained. With the simulated time histories in hand, one can readily plot a dimensionless root of mean square (RMS) displacement versus reduced velocity curve as shown in Fig. 3. The RMS response is normalized by D, the diameter of the tube, and is expressed in percentage. We calculate RMS response from 0 to 30 seconds. This RMS response curve is attainable in experiment, and also plotted in Fig. 3 is the experimental results by Weaver and Parrondo in 1991 [56]. The measured critical reduced velocity in the experiment is 17.2, very close to our simulation result 18.57. The simulated RMS response by our SATD model agrees surprisingly well with the response reported by Weaver and Parrondo [56].

The FEI instability concerned herein is classified into the damping-controlled instability. Identifying and unveiling the role of the damping and frequency is crucial for understanding the underlying physics of the instability. It is very easy to calculate the free vibration response of the system by using the time-domain model, from which an equivalent damping can be obtained following a routine logarithmic decrement technique. The period and thus the frequency are also determined accordingly. Fig. 4 plots the vibration of the equivalent damping coefficient and the circular frequency ratio, ω/ω_n, with reduced velocity, U_r. Here, ω is the vibration frequency and ω_n is the natural frequency. The damping coefficient versus reducing velocity curve in Fig. 4(a) clearly reveals the damping-controlled mechanism: When the velocity is below the critical velocity, $U_r^c=18.57$, the equivalent damping of

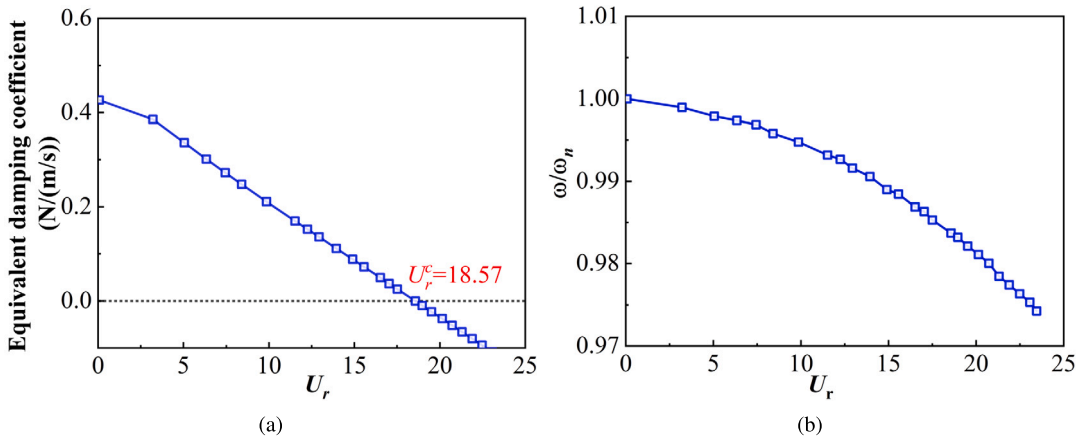

Fig. 4. The result of the parallel triangular tube array with a pitch ratio of 1.47 (a) The equivalent damping coefficient versus different reduced velocities U_r (b) The frequency ratio at different reduced velocities U_r.

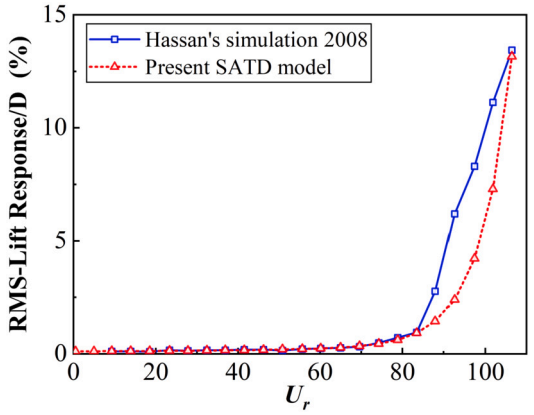

Fig. 5. Comparison of Hassan's simulation for a in-line square array with pitch ratio 1.5 (blue line) and simulation of present SATD model (red dash line).

the system is positive and thus the system is stable; when the velocity is greater than the critical velocity, the system exhibits negative damping and is unstable. The intersection of the equivalent damping with the horizontal zero damping line (dotted line) determines the critical velocity, $U_r^c = 18.57$. The frequency ratio versus reduced velocity in Fig. 4(b) shows a monotonically decreasing trend with increasing reduced velocity $\omega/\omega_n = 1$ at $U_r = 0$, which indicates that the vibration frequency deviates from natural frequency with increasing velocity. This is attributed to the fact that the fluid-structure interaction and the added mass effect become more profound with the increase of velocity.

The time-domain FEI analysis mentioned above can be applied for other tube array configurations with various pitch ratios. The table in the Appendix A collects four array configurations widely adopted in real engineering designs as well as the parameters used. For the purpose of demonstration, Fig. 5 presents the RMS response for an in-line square tube array with pitch ratio 1.5 and MDP 60. Also included is the time-domain analysis results by Hassan et al. [43] for comparison. From Fig. 5, it is readily to estimate the critical reduced velocity as $U_r^c = 77.45$, which is very close to Hassan's result. Fig. 6(a) and Fig. 6(b) plot the equivalent damping coefficient and frequency ratio versus reduced velocity curves for the in-line square array case, and they show similar behavior as those in Fig. 4.

Our new formulations derived the explicit fluid force expressions analytically. The explicit fluid force associated with current displacement, velocity and acceleration can be incorporated easily into structural vibration equations and a routine Galerkin discretization procedure as discussed in Section 2.3.2 can be performed. This coefficient-based form facilitates the analysis of a continuous beam subjected to crossflow. We choose a single-span straight beam as a numerical example, and the parameters used for simulation are summarized as follows: $p_r = 1.47$, MDP = 17.35, $\delta = 0.04$, $D = 0.0126$ m, $f_n = 63.5$ Hz. For the problem considered here, the RMS of the dynamic response is similar to that in Fig. 3 and Fig. 5 and the details are omitted here. The critical velocity for FEI of this single-span straight beam is $U_r{}^c = 19$. In the literature, the time-domain FEI analysis results are very limited and some parameters are missing, which hinders researchers from reproducing some fundamental results. We believe in that our results presented here in together with the detailed parameters provided constitute a benchmark problem for truly time-domain FEI analysis.

The SATD model also allows us to perform a frequency-domain FEI analysis in a consistent way, which is straightforward by restoring the harmonic solution assumption and following the procedure described in Section 2.4. FEI threshold values or the stability

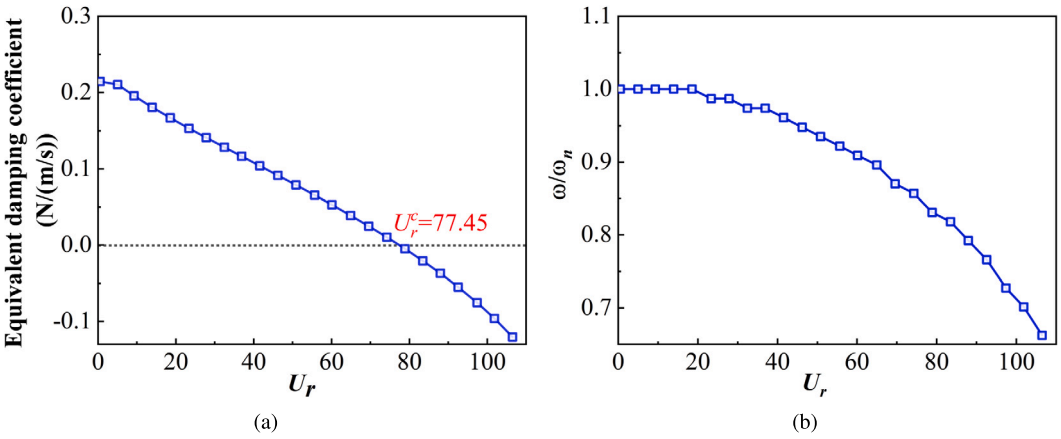

Fig. 6. The result of the in-line square tube array with a pitch ratio of 1.5 (a) The equivalent damping coefficient versus different reduced velocities U_r (b) The frequency ratio at different reduced velocities U_r.

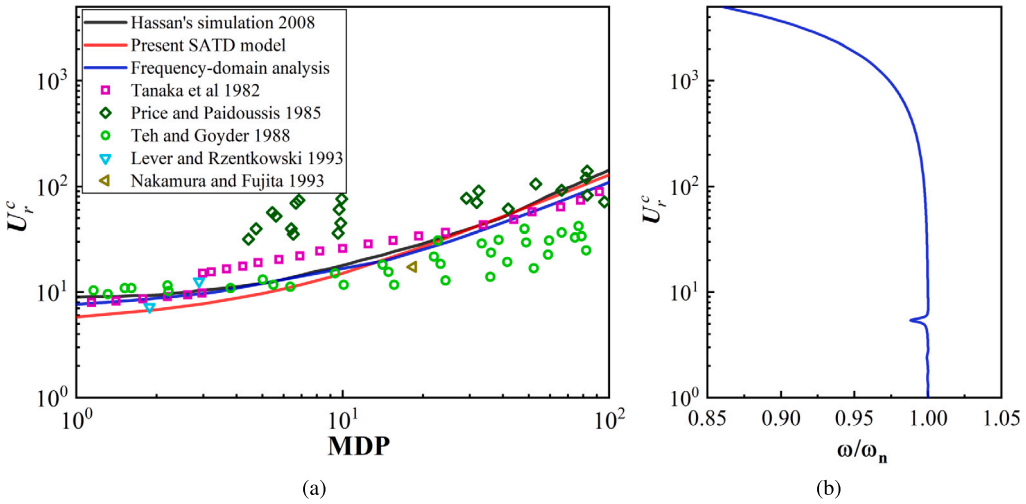

Fig. 7. Comparison of stability thresholds obtained by current SATD model and other model and available experimental data. (a) Stability plot comparing present theoretical threshold curves obtained by frequency-domain (blue line) and time-domain (red line) analysis to existing experimental data. (b) Critical reduced velocity versus frequency ratio curve.

diagram, which is of utmost importance in engineering, can thus be attained either from a frequency-domain analysis or from a time-domain analysis. Fig. 7 (a) plots the critical reduced velocity versus MDP curve obtained from our model for an in-line square array with $P_r = 1.5$. Comparison is made against other analysis results and experimental data reported in literature [57–61]. The red solid line in Fig. 7 (a) is the result by performing a time-domain analysis using SATD model for an SDOF system. The blue line in the figure is the result obtained by performing a frequency-domain analysis using our model. The black solid line is the time-domain FEM result by Hassan for a cantilever beam [43]. Various markers in Fig. 7 (a) are experimental data taken from literature. Fig. 7 (a) indicates that our time-domain and frequency-domain analysis results agree well with the time-domain FEM result by Hassan, and correlates well with experimental data. As described in Section 2.4, the vibration frequency is unknown a priori and can be obtained in an iterative way. Fig. 7 (b) plots the critical reduced velocity versus dimensionless frequency ratio. Note that for low velocity the vibration frequency is very close to the natural frequency of the system, and it gradually deviates from the natural frequency with increasing critical velocity.

4. Nonlinear dynamics of a loosely-supported tube in crossflow

Fig. 2 (b) shows the schematic of a loosely supported cylinder. The surrounding rigid tubes are omitted here, and the illustration of the whole tube array as well as the stream tubes are referred to Fig. 1. The location of the loose support occurs at $x = x_b$ with gap denoted by d. For the purpose of simplicity and illustration of new model, the problem considered here is a single-span beam with only one loose support. But our theory is generic and applicable for single-span tube with multiple supports and multi-span tube even U-tubes without difficulties. The cylinder has a length L and is subjected to a uniform fluid force denoted by F_L. The detailed

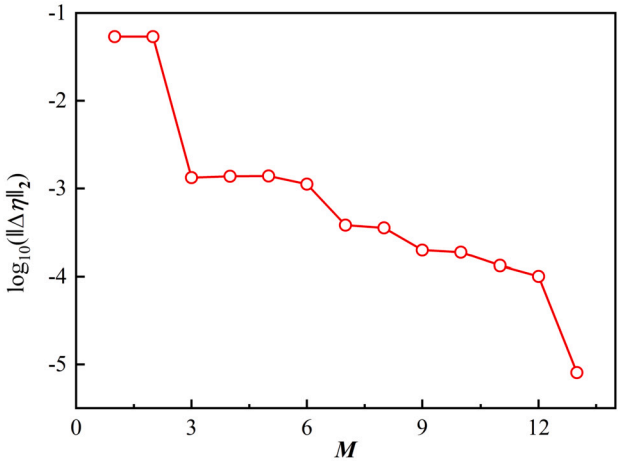

Fig. 8. Convergence of the logarithm of the L_2-norm of solution errors with increasing number of truncated vibration modes for reduced velocity $U_r = 20$.

formulation of the fluid force is provided in Section 2.2. The motion of the cylinder can be described by the beam vibration equation as

$$m\frac{\partial^2 w}{\partial t^2} + c\frac{\partial w}{\partial t} + EI\frac{\partial^4 w}{\partial x^4} + \delta(x - x_b)f(w) = F_L \tag{42}$$

All the physical quantities as well as the equations are normalized and given in the dimensionless forms. Details of normalization are found in Section 2.3.2. A dimensionless form of Eq. (42) is written as

$$\left(1 - \tilde{m}_{FE}\right)\frac{\partial^2 \eta}{\partial \tilde{t}^2} + \left(\zeta - \tilde{c}_{FE}\right)\frac{\partial \eta}{\partial \tilde{t}} + \frac{1}{{\lambda_1}^4}\frac{\partial^4 \eta}{\partial \xi^4} - \tilde{k}_{FE}\eta + \delta(\xi - \xi_b)\tilde{f}(\eta) = \tilde{F}_{td}\left(\eta(\tilde{t} - \tilde{\tau}), \dot{\eta}(\tilde{t} - \tilde{\tau}), \ddot{\eta}(\tilde{t} - \tilde{\tau})\right) \tag{43}$$

where the nonlinear property of the loose support is approximated by the following piece-wise stiffness

$$\tilde{f}(\eta) = \kappa\left[\eta - \frac{1}{2}\left(|\eta + \tilde{d}| - |\eta - \tilde{d}|\right)\right] \tag{44}$$

The piece-wise stiffness, Eq. (44), is non-smooth and thus more accurate than the cubic spring model. The partial differential equation (PDE) in Eq. (42) can be transformed into a set of ordinary differential equations (ODE) by using the mode truncation technique and the Galerkin discretization described in Section 2.3.2. The resultant ODEs with various time delay can be solved by a MATLAB function ddensd or by coding a home-made solver, such as a Newmark integration, for delay differential equations (DDEs) [42].

Regarding the mode truncation technique used for approximation and discretization, an issue worth mentioning is the number of truncated vibration modes. The number of modes requested is determined through a convergence study and the result is presented in Fig. 8. It plots the logarithm of L_2 norm of errors versus number of natural modes. The L_2 norm is obtained by evaluating the error of a solution for a selected number of modes with that for a pretty large number of modes, which gives a true solution as expected. Fig. 8 indicates that five orders of modes are sufficient to give results with reasonable accuracy, about 10^{-3} in terms of L_2 error. The number of truncated modes is thus fixed to be five in all following simulations.

Fig. 9 plots time histories of response of the system at a range of reduced velocities, i.e., U_r = 18.75, 19, 21.5, 30, and 45, respectively. All the displacements plotted here, denoted by η_b in Fig. 9, are measured at the midpoint of the beam where the loose support with gap $\tilde{d} = 0.002$, dimensionless stiffness coefficient of the piece-wise linear spring $\kappa = 5000$ is enforced. At U_r = 18.75, the system exhibits convergent response with amplitude much smaller than the clearance, and therefore no contact occurs. Fig. 9 indicates that the critical velocity for the onset of FEI is U_r = 19. Beyond the critical velocity, the system undergoes severe FEI vibration. However, the presence of gap levels off the vibration amplitudes and results in contact between the tube and the support. With increase of flow velocity, say U_r = 45, the wave profile is distorted by contacts as can be seen from the localized region around the peak.

The simple time history presented in Fig. 9 can only determine the stable or unstable behavior of the system. It is difficult to probe critically the periodic, quasi-periodic or chaotic behavior of the system only based on these time histories. Recourse is thus made by plotting phase portraits, Poincaré maps and the power spectral densities (PSD), which are presented in Fig. 10 for various reduced velocities. In Fig. 10, the left panels are the phase portraits, the middle panels are the Poincaré maps, and the right panels are the corresponding PSD curves. The phase portraits imply that at velocity near the critical velocity the shape of the phase portrait is nearly an ellipse, but the nearly ellipse-shaped phase portraits are distorted with increasing velocity. The impact between the tube and the support is responsible for the distortion.

The Poincaré map is a powerful approach to distinguish chaotic response from periodic or quasi-periodic responses. For an autonomous system, one must choose a super-plane to obtain the Poincaré map. Following Cai and Chen [51], we chose the plane, say when $\eta(0.2, t) = 0$ and $\dot{\eta}(0.2, t) > 0$, at which the values of $\eta(0.5, t)$ and $\dot{\eta}(0.5, t)$ were saved. The Poincaré maps indicate that

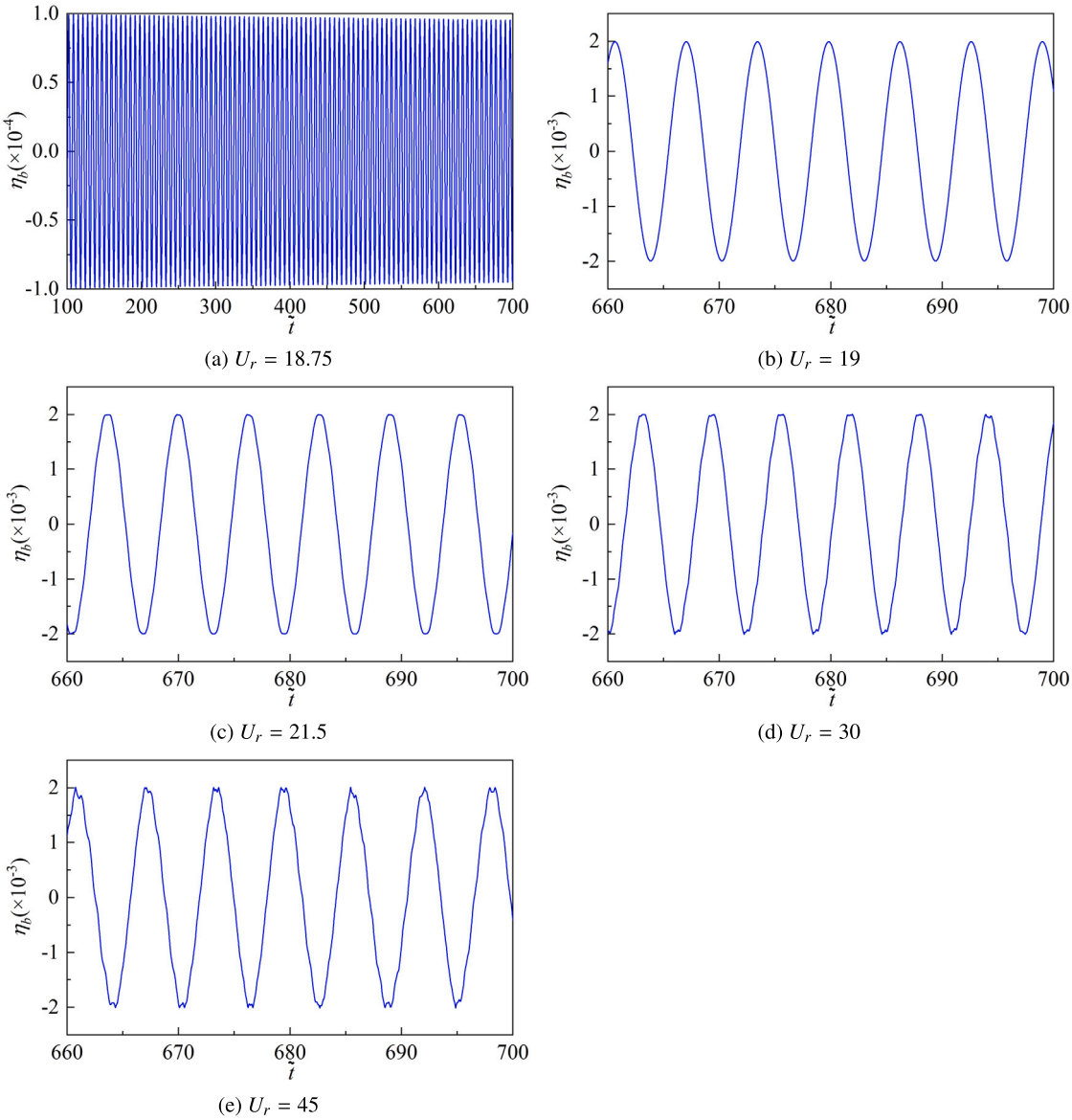

Fig. 9. Time history of the midpoint of the tube under various reduced velocities.

no exactly periodic solutions exist in the system, even for low velocity at $U_r = 19$. The Poincaré maps in Fig. 10 (b) and Fig. 10 (e) corresponding to $U_r = 19$ and 21.5 are narrow strips instead of a single fixed point in an exactly periodic system. This means that the response is nearly but not exactly periodic. If the velocity is further increased, say $U_r = 30$ and 45 in Fig. 10 (h) and (k), the Poincaré maps turn into clouds of scattered points, indicating that the response is chaotic. As velocity is increased from 30 to 45, the basin of Poincaré points becomes more scattered and the boundary of the basin becomes more non-smooth and even fractal [62,63].

Besides phase plane portraits and Poincaré maps, the PSD curves can also distinguish periodic signals from chaotic ones from the perspective of frequency domain. The right panels in Fig. 10, i.e., Fig. 10 (c), (f), (i), and (l), plots the PSDs of displacement at various reduced velocities. Note that the largest peaks of all these curves remain the same, i.e., $f_1 =$ 0.1578 Hz, so that the frequencies in these PSD curves are normalized by f_1 and can be given by dimensionless number. At $U_r = 19$, the PSD have four discrete peaks located at $f/f_1 = 1$, 2, 3 and 4 as shown in Fig. 10 (c). The peaks corresponding to integer multiples of the fundamental frequency are identified as superharmonic components. Since all the peaks of PSD in Fig. 10 (c) occur at frequencies commensurable with the fundamental frequency, the vibration is nearly periodic. At $U_r = 21.5$, the nearly periodic vibration changes to quasi-periodic. A range of discrete peaks could be found in Fig. 10 (f), whereby two periodic oscillations take place simultaneously at two incommensurable fundamental frequencies, i.e., $f_1 = 0.1578$ Hz and $f_2 = 0.1989$ Hz, and the frequencies of the pronounced peaks are a combination of these incommensurable frequencies, i.e., $f = nf_1 + mf_2$. Fig. 10 (f) shows the corresponding combination of the two fundamental

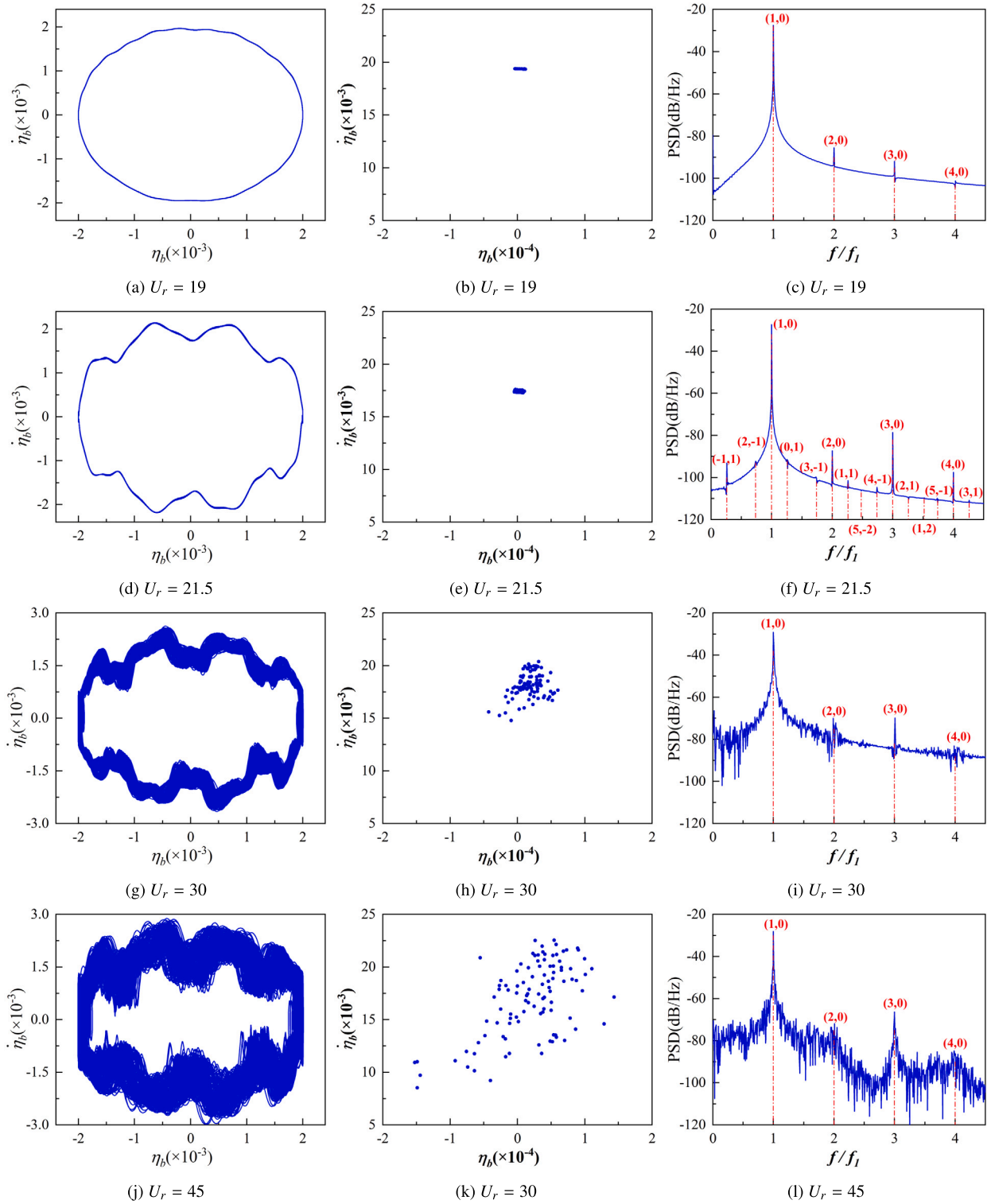

Fig. 10. Phase portraits (left panel), Poincaré maps (middle panels), and PSD (right panels) of the system for various reduced velocites. (a)-(c) $U_r = 19$ (d)-(f) $U_r = 21.5$ (g)-(i) $U_r = 30$ (j)-(l) $U_r = 45$.

frequencies. When the velocity is increased to 30 and 45, the PSDs demonstrate characteristic limited-band chaos, although the fundamental frequencies are still discernible.

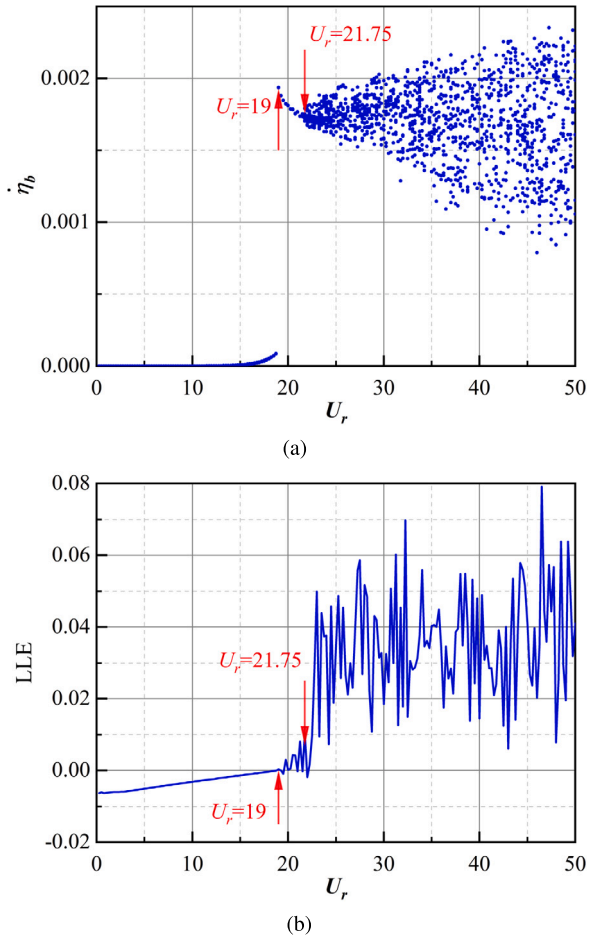

Fig. 11. The bifurcation diagram (a) and the largest Lyapunov exponents (LLE) (b) extracted at the midpoint of tube versus the reduced velocity.

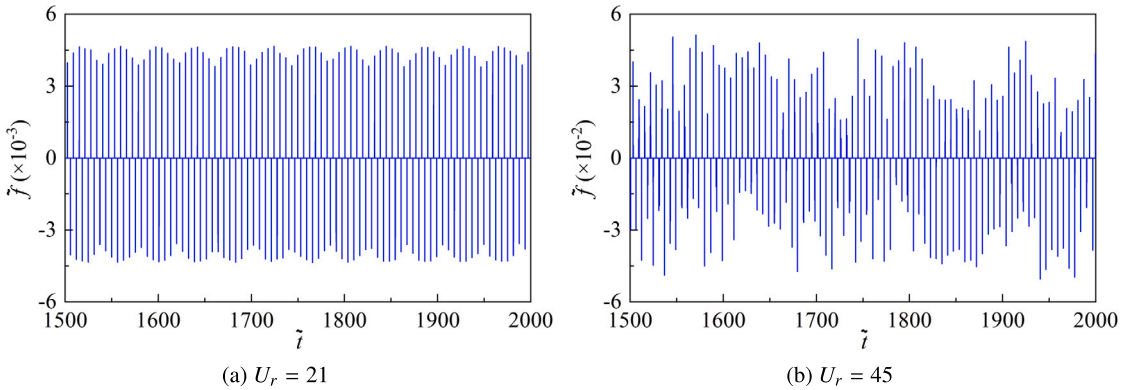

Fig. 12. Time history of the impact force measured at the loose support.

To further probe the nonlinear dynamics in a quantitative way, and in particular to investigate the routes to chaos for such a system, Fig. 11 plots the bifurcation diagram together with the largest Lyapunov exponent (LLE) as reduced velocity varies. We use the small data sets algorithm to calculate the LLE with the MATLAB function lyapunovExponent. The LLE quantitatively characterizes the nonlinear dynamics of the system: When the LLE is negative for $U_r < 19$, the vibration is convergent; When the LLE is positive for $U_r > 21.75$, the vibration is chaotic; for $19 < U_r < 21.75$, the LLE oscillates around a small but positively biased average value, and the system is quasi-periodic. The bifurcation diagram in Fig. 11 (a) plots the velocity of the midpoint of the beam when $\eta(0.5,t) = 0$ and $\dot{\eta}(0.5,t) > 0$ versus the reduced velocity. The transitions of stable to quasi-periodic and ultimately chaotic vibrations coincide

well with that in Fig. 11 (b). Fig. 12 plots two impact force histories for $U_r = 21$ and $U_r = 45$, respectively, the former is nearly periodic and the latter is chaotic as expected. For different flow velocities, the level of the impacting force almost remains the same.

5. Concluding remarks

Flow-induced vibration (FIV) is one of the major sources of failure of components in steam generators and heat exchangers, in particular the numerous loosely supported tubes subjected to crossflow. Among several FIV mechanisms of tube bundles, the fluidelastic instability (FEI) is widely acknowledged as the greatest concern, since it has the potential to cause large amplitude vibration when the flow velocity is beyond the critical velocity. This in turn causes severe damage of tubes. Developing theoretical models for FEI remains a sought-after task which has been impaired due to the complexity of FEI, in particular the multi-phase unsteady flow as well as fluid and structural nonlinearity. Despite some progress, there is still a long way to go to develop a general FEI model that is suitable and reasonably accurate for all tube array patterns and all possible flow conditions. Previous efforts on FEI model development have been devoted to linear FEI stability analysis, which was typically completed in frequency-domain. Few attempts were made to carry out truly time-domain nonlinear response analysis. This is vital for fretting-wear simulation, which heavily depends on detailed tube response and tube/support interaction history.

It is highly desirable to develop semi-analytical models, which utilize some basic principles and analytical derivations but also rely on some experimental parameters, to understand and interpret phenomena observed in experiments. The semi-analytical model originally proposed by Lever and Weaver in 1980s is such a semi-analytical model that requires fewer experimental inputs as compared to other FEI models, such as the unsteady model and the quasi-steady model. The original Lever and Weaver model was mainly used for frequency-domain stability analysis, aiming at obtaining critical velocity and the stability plot for engineering design. This model was recently extended by Hassan et al. for truly time-domain nonlinear analysis. They successfully demonstrated that the time-domain model and the numerical tool can model time history of loosely supported multi-span tubes and U-tubes. The derivation and in particular the implementation of the semi-analytical model is more complicated and hard to achieve compared with the unsteady and the quasi-steady model. The reason is obvious: In the unsteady model and the quasi-steady model, the fluid force expressions are explicit in terms of vibration responses and given in a coefficient form. The explicit fluid force expressions ease the implementation of the unsteady and the quasi-steady model; in the semi-analytical model, on the other hand, it is hard to derive an explicit fluid force expression though not prohibitive. The fluid force in the semi-analytical model is expressed as a black-box integral form. This hinders the understanding and application of the semi-analytical model. The issue becomes more profound especially in time-domain analysis, where the simple harmonic solution assumption adopted in frequency-domain analysis is discarded. The implementation of the semi-analytical model in time domain remains a mystery, even in the community of FIV researchers.

Here, we present a new formulation of the semi-analytical time-domain (SATD) FEI model for tube bundles subjected to crossflow. We follow exactly the same assumptions and unsteady fluid equations adopted in the original semi-analytical model. We integrate the integral of the fluid force analytically and differentiate the terms associated with current vibration response from the terms with time-delay. We attain explicit fluid force expressions, albeit in an integral form. After some analytical derivations, fluid force terms related to current response are expressed as mass, damping and stiffness terms with coefficients given by single definite integrals. All this was done in a closed-form. The outcome is an explicit expression for fluid force associated with current responses plus some integrals associated with the responses at previous instants. The former can be combined together with structural mass, damping and stiffness terms, while the latter could be computed numerically and stored as a load vector. The new formulations entail a coefficient-based explicit fluid force expression for the semi-analytical model, which has long been thought impossible in time-domain analysis, where the simple harmonic assumption does not hold. Our findings resolve a long-standing issue about the possibility of expressing fluid force analytically in a coefficient-based form, the same as that in the unsteady model and the quasi-static model. With the new formulation in hand, we show that a consistent FEI analysis, either frequency-domain or time-domain, is possible and can be derived from the same set of equations, which is reasonable and ought to be the case. The frequency-domain analysis is only a special case by invoking the harmonic solution assumption. In literature, the frequency-domain stability analysis and the time-domain response analysis are parallel and are not treated in such a consistent way. Furthermore, our formulations for frequency-domain analysis work for arbitrary piece-wise decay and delay functions, and formulation does not change when the decay or delay functions are changed. The frequency-domain stability analysis and the threshold values obtained through time-domain analysis coincides with each other, and agrees well with available experimental data, for both parallel triangle tube array and in-line square array. Our new theory facilitates the implementation of SATD FEI analysis in either of the numerical frameworks, such as finite element method, finite difference method, mode truncation method, etc. These results are beyond the scope of the current paper and will be reported elsewhere. Furthermore, the incorporation of nonlinear boundary effect or other structural nonlinearity is straightforward and the load vectors from nonlinearity and that from time-delayed fluid force terms are summed up to form the global load vectors. This means that the formulation of the whole theory is not altered when modeling the nonlinear dynamics of loosely supported tubes in crossflow.

The studies on the nonlinear post-instability dynamics of loosely supported tubes are very limited and sparse in literature. The frequent occurrence of FIV induced fretting wear and fatigue damage of steam generator and heat exchanger tubes calls for detailed response analysis of elastic tubes in crossflow. This has, however, been impaired by the complexity of coupled structural nonlinearity and fluidelastic interaction, as well as by the lack of appropriate time-domain models for FEI. Yet, the limited studies on nonlinear time-domain FEI analysis of loosely supported tubes have been performed by employing the simple Connor's quasi-static model, the quasi-steady model, and the unsteady model. Fruitful nonlinear phenomena, such as bifurcation and chaos, have been successfully

captured. In the context of the semi-analytical model, nevertheless, no efforts have been conducted toward this direction and only simple time traces of response were reported. It is highly desirable to probe nonlinear dynamics of loosely supported tubes in the context of the semi-analytical time-domain (SATD) model.

Based on the new theory of SATD model, this paper provides the first reference on the nonlinear dynamics of a single loosely supported tube in an otherwise rigid tube array. The loose support is modeled as a piece-wise linear spring. Various measures have been utilized to characterize the nonlinear behavior of the system, including time history, phase portrait, Poincaré map, PSD, bifurcation diagram, and the largest Lyapunov exponent. In depth analysis was performed on the various aspects of characterizations, and excellent agreement was achieved. The various characterizations unveil that there exist two critical velocities, one for the onset of FEI instability and another for transition from quasi-periodic solution to chaos. Our analysis thus elucidates that the route to chaos is through a quasi-periodic to chaotic transition. Our efforts enrich the current FEI theory, and open an avenue for nonlinear time-domain response analysis of steam generator tubes.

Finally, we should admit that our formulations with explicit fluid force expressions are derived from an ideal scenario where a flexible tube is surrounded by a rigid tube array and subjected to single-phase crossflow. For tube array with fully flexible tubes, explicit fluid force expressions are not available due to the complexity of inter-tube interaction. Moreover, our current SATD model and the original semi-analytical model are semi-analytical in the sense that the determination of decay function and in particular the time-delay or phase lag function relies on experiments or high-fidelity CFD simulations. It is highly desirable to develop analytical expressions for phase lag functions, rendering the model purely analytical. The work by Benaouicha et al. [64] on deriving an algebraic phase lag model from the potential theory, and the work by Alyaldin and Mureithi [65] on analytical frequency response function and time delay function, are works in this direction.

Declaration of competing interest

The authors declare that they have no known competing financial interests or personal relationships that could have appeared to influence the work reported in this paper.

Data availability

No data was used for the research described in the article.

Acknowledgement

This research is supported by National Natural Science Foundation of China (grant 11972277) and by Science and Technology on Reactor System Design Technology Laboratory (LRSDT2021205).

Appendix A

The geometric parameters of the SATD model for various tube arrays are shown in Table 1.

Table 1
System parameters for various arrays as used in the present model; $s_a = -\beta_1 D/2$, $s_s = -\beta_2 D/2$, $N_{row} = 1.5$.

Configuration	α	A_0	s_0	β_1	β_2
In-line square	0°	$\left(P_r - 1\right) D$	$P_r N_{row} D$	10°	10°
Parallel triangle	30°	$\left(P_r - 1\right) D$	$P_r \alpha N_{row} D$	40°	10°
Rotated square ($P_r \le 1.7$)	45°	$\left(P_r - 1\right) D$	$P_r \alpha N_{row} D$	75°	15°
Rotated square ($P_r > 1.7$)	45°	$\left(P_r \cos\alpha - 0.5\right) D$	$\frac{P_r[\alpha+\sin\alpha]}{2} N_{row} D$	85°	15°
Rotated triangle	60°	$\left(P_r \cos\alpha - 0.5\right) D$	$\frac{P_r[\alpha+\sin\alpha]}{2} N_{row} D$	85°	15°

Appendix B

The derivation of the five-term fluid force expression of Eq. (19) in Section 2.2 is given below:
The first term:

$$\frac{2\rho {U_0}^2}{A_0} \int_{-s_a}^{s_s} a(s,t) \cdot \cos\beta(s) ds = \frac{2\rho {U_0}^2}{A_0} \int_{-s_a}^{s_s} \cos\beta(s) ds \cdot w(t) \tag{B.1}$$

The second term:

$$\begin{aligned}\frac{4\rho U_0}{A_0}\int_{-s_a}^{s_s}\cos\beta(s)\int_{-s_0}^{s}\dot{a}(s,t)\,ds_1ds&=\frac{4\rho U_0}{A_0}\left[\int_{-s_a}^{s_s}\cos\beta(s)\int_{-s_0}^{-s_a}\dot{a}(s,t)\,ds_1ds+\int_{-s_a}^{s_s}\cos\beta(s)\int_{-s_a}^{s}\dot{a}(s,t)\,ds_1ds\right]\\&=\frac{4\rho U_0}{A_0}\left[\int_{-s_a}^{s_s}\cos\beta(s)\int_{-s_0}^{-s_a}\dot{w}[t\text{-}\tau(s_1)]\gamma(s_1)\,ds_1ds+\int_{-s_a}^{s_s}\cos\beta(s)\int_{-s_a}^{s}ds_1ds\cdot\dot{w}(t)\right]\end{aligned}\tag{B.2}$$

The third term:

$$\begin{aligned}\frac{2\rho}{A_0}\int_{-s_a}^{s_s}\cos\beta(s)\int_{-s_0}^{s}\int_{-s_0}^{s_1}\ddot{a}(s,t)\,ds_2ds_1ds&=\frac{2\rho}{A_0}\left[\int_{-s_a}^{s_s}\cos\beta(s)\int_{-s_0}^{-s_a}\int_{-s_0}^{s_1}\ddot{a}(s,t)\,ds_2ds_1ds+\int_{-s_a}^{s_s}\cos\beta(s)\int_{-s_a}^{s}\int_{-s_0}^{-s_a}\ddot{a}(s,t)\,ds_2ds_1ds\right.\\&\left.+\int_{-s_a}^{s_s}\cos\beta(s)\int_{-s_a}^{s}\int_{-s_a}^{s_1}\ddot{a}(s,t)\,ds_2ds_1ds\right]\\&=\frac{2\rho}{A_0}\left[\int_{-s_a}^{s_s}\cos\beta(s)\int_{-s_0}^{-s_a}\int_{-s_0}^{s_1}\ddot{w}[t\text{-}\tau(s_2)]\gamma(s_2)\,ds_2ds_1ds\right.\\&+\int_{-s_a}^{s_s}\cos\beta(s)\int_{-s_a}^{s}\int_{-s_0}^{-s_a}\ddot{w}[t\text{-}\tau(s_2)]\gamma(s_2)\,ds_2ds_1ds\\&\left.+\int_{-s_a}^{s_s}\cos\beta(s)\int_{-s_a}^{s}\int_{-s_a}^{s_1}ds_2ds_1ds\cdot\ddot{w}(t)\right]\end{aligned}\tag{B.3}$$

The fourth term:

$$\begin{aligned}\frac{2\rho hU_0{}^2}{A_0s_0}\int_{-s_a}^{s_s}\cos\beta(s)\int_{-s_0}^{s}a(s,t)\,ds_1ds&=\frac{2\rho hU_0{}^2}{A_0s_0}\left[\int_{-s_a}^{s_s}\cos\beta(s)\int_{-s_0}^{-s_a}a(s,t)\,ds_1ds+\int_{-s_a}^{s_s}\cos\beta(s)\int_{-s_a}^{s}a(s,t)\,ds_1ds\right]\\&=\frac{2\rho hU_0{}^2}{A_0s_0}\left[\int_{-s_a}^{s_s}\cos\beta(s)\int_{-s_0}^{-s_a}w[t\text{-}\tau(s_1)]\gamma(s_1)\,ds_1ds+\int_{-s_a}^{s_s}\cos\beta(s)\int_{-s_a}^{s}ds_1ds\cdot w(t)\right]\end{aligned}\tag{B.4}$$

The fifth term:

$$\begin{aligned}\frac{2\rho hU_0}{A_0s_0}\int_{-s_a}^{s_s}\cos\beta(s)\int_{-s_0}^{s}\int_{-s_0}^{s_1}\dot{a}(s,t)\,ds_2ds_1ds&=\frac{2\rho hU_0}{A_0s_0}\left[\int_{-s_a}^{s_s}\cos\beta(s)\int_{-s_0}^{-s_a}\int_{-s_0}^{s_1}\dot{a}(s,t)\,ds_2ds_1ds\right.\\&+\int_{-s_a}^{s_s}\cos\beta(s)\int_{-s_a}^{s}\int_{-s_0}^{-s_a}\dot{a}(s,t)\,ds_2ds_1ds\\&\left.+\int_{-s_a}^{s_s}\cos\beta(s)\int_{-s_a}^{s}\int_{-s_a}^{s_1}\dot{a}(s,t)\,ds_2ds_1ds\right]\\&=\frac{2\rho hU_0}{A_0s_0}\left[\int_{-s_a}^{s_s}\cos\beta(s)\int_{-s_0}^{-s_a}\int_{-s_0}^{s_1}\dot{w}[t\text{-}\tau(s_2)]\gamma(s_2)\,ds_2ds_1ds\right.\\&+\int_{-s_a}^{s_s}\cos\beta(s)\int_{-s_a}^{s}\int_{-s_0}^{-s_a}\dot{w}[t\text{-}\tau(s_2)]\gamma(s_2)\,ds_2ds_1ds\\&\left.+\int_{-s_a}^{s_s}\cos\beta(s)\int_{-s_a}^{s}\int_{-s_a}^{s_1}ds_2ds_1ds\cdot\dot{w}(t)\right]\end{aligned}\tag{B.5}$$

Summing up the above five items, and separating terms associated with current response from those with time delay, the fluid force in Eq. (19) can be written as:

$$
\begin{aligned}
F_L =& \frac{2\rho}{A_0}\int_{-s_a}^{s_s}\cos\beta(s)\int_{-s_a}^{s}\int_{-s_a}^{s_1} ds_2 ds_1 ds\cdot\ddot{w}(t)\\
&+\frac{4\rho U_0}{A_0}\int_{-s_a}^{s_s}\cos\beta(s)\int_{-s_a}^{s} ds_1 ds\cdot\dot{w}(t)+\frac{2\rho h U_0}{A_0 s_0}\int_{-s_a}^{s_s}\cos\beta(s)\int_{-s_a}^{s}\int_{-s_a}^{s_1} ds_2 ds_1 ds\cdot\dot{w}(t)\\
&+\frac{2\rho {U_0}^2}{A_0}\int_{-s_a}^{s_s}\cos\beta(s) ds\cdot w(t)+\frac{2\rho h {U_0}^2}{A_0 s_0}\int_{-s_a}^{s_s}\cos\beta(s)\int_{-s_a}^{s} ds_1 ds\cdot w(t)\\
&+\int_{-s_a}^{s_s}\cos\beta(s)\int_{-s_0}^{-s_a}\left[\frac{4\rho U_0}{A_0}\dot{w}\left[t\text{-}\tau(s_1)\right]+\frac{2\rho h {U_0}^2}{A_0 s_0} w[t\text{-}\tau(s_1)]\right]\gamma(s_1)\, ds_1 ds\\
&+\int_{-s_a}^{s_s}\cos\beta(s)\int_{-s_0}^{-s_a}\int_{-s_0}^{s_1}\left[\frac{2\rho}{A_0}\ddot{w}[t\text{-}\tau(s_2)]+\frac{2\rho h U_0}{A_0 s_0}\dot{w}[t\text{-}\tau(s_2)]\right]\gamma(s_2)\, ds_2 ds_1 ds\\
&+\int_{-s_a}^{s_s}\cos\beta(s)\int_{-s_a}^{s}\int_{-s_0}^{-s_a}\left[\frac{2\rho}{A_0}\ddot{w}[t\text{-}\tau(s_2)]+\frac{2\rho h U_0}{A_0 s_0}\dot{w}[t\text{-}\tau(s_2)]\right]\gamma(s_2)\, ds_2 ds_1 ds\\
=&\alpha_2\int_{-s_a}^{s_s}\cos\beta(s)\cdot\frac{\left(s+s_a\right)^2}{2} ds\cdot\ddot{w}(t)\\
&+\int_{-s_a}^{s_s}\cos\beta(s)\cdot\left[\alpha_1\left(s+s_a\right)+\frac{\alpha_4\left(s+s_a\right)^2}{2}\right] ds\cdot\dot{w}(t)\\
&+\int_{-s_a}^{s_s}\cos\beta(s)\cdot\left[\alpha_5+\alpha_3\left(s+s_a\right)\right] ds\cdot w(t)\\
&+\int_{-s_a}^{s_s}\cos\beta(s)\int_{-s_0}^{-s_a}\left\{\alpha_1\dot{w}[t\text{-}\tau(s_1)]+\alpha_3 w[t\text{-}\tau(s_1)]\right\}\gamma(s_1) ds_1 ds\\
&+\int_{-s_a}^{s_s}\cos\beta(s)\int_{-s_0}^{-s_a}\int_{-s_0}^{s_1}\left\{\alpha_2\ddot{w}[t\text{-}\tau(s_2)]+\alpha_4\dot{w}[t\text{-}\tau(s_2)]\right\}\gamma(s_2) ds_2 ds_1 ds\\
&+\int_{-s_a}^{s_s}\cos\beta(s)\int_{-s_a}^{s}\int_{-s_0}^{-s_a}\left\{\alpha_2\ddot{w}[t\text{-}\tau(s_2)]+\alpha_4\dot{w}[t\text{-}\tau(s_2)]\right\}\gamma(s_2) ds_2 ds_1 ds
\end{aligned}
\tag{B.6}
$$

Where α_1, α_2, α_3, α_4 and α_5 are constants and defined as

$$
\alpha_1=\frac{4\rho U_0}{A_0},\qquad \alpha_2=\frac{2\rho}{A_0},\qquad \alpha_3=\frac{2\rho {U_0}^2}{A_0 s_0},\qquad \alpha_4=\frac{2\rho h U_0}{A_0 s_0},\qquad \alpha_5=\frac{2\rho {U_0}^2}{A_0}
$$

The first three terms of the fluid force in Eq. (B.6) are fluid force without time delay, and are defined as mass, damping and stiffness terms respectively:

$$
m_{FE}=\frac{2\rho}{A_0}\int_{-s_a}^{s_s}\cos\beta(s)\int_{-s_a}^{s}\int_{-s_a}^{s_1} ds_2 ds_1 ds=\alpha_2\int_{-s_a}^{s_s}\cos\beta(s)\cdot\frac{\left(s+s_a\right)^2}{2} ds \tag{B.7}
$$

$$\begin{aligned} c_{FE} &= \frac{4\rho U_0}{A_0}\int_{-s_a}^{s_s}\cos\beta(s)\int_{-s_a}^{s} ds_1 ds + \frac{2\rho h U_0}{A_0 s_0}\int_{-s_a}^{s_s}\cos\beta(s)\int_{-s_a}^{s}\int_{-s_a}^{s_1} ds_2 ds_1 ds \\ &= \int_{-s_a}^{s_s}\cos\beta(s)\cdot\left[\alpha_1\left(s+s_a\right)+\frac{\alpha_4\left(s+s_a\right)^2}{2}\right]ds \end{aligned} \tag{B.8}$$

$$\begin{aligned} k_{FE} &= \frac{2\rho {U_0}^2}{A_0}\int_{-s_a}^{s_s}\cos\beta(s)\,ds + \frac{2\rho h {U_0}^2}{A_0 s_0}\int_{-s_a}^{s_s}\cos\beta\int_{-s_a}^{s} ds_1 ds \\ &= \int_{-s_a}^{s_s}\cos\beta(s)\cdot\left[\alpha_5+\alpha_3\left(s+s_a\right)\right]ds \end{aligned} \tag{B.9}$$

Substituting Eq. (B.7)-(B.9) into Eq. (B.6), the final explicit coefficient-based form of the fluid force is derived:

$$\begin{aligned} F_L =& m_{FE}\ddot{w}(t) + c_{FE}\dot{w}(t) + k_{FE}w(t) \\ &+ \int_{-s_a}^{s_s}\cos\beta(s)\int_{-s_0}^{-s_a}\left\{\alpha_1\dot{w}[t\text{-}\tau(s_1)]+\alpha_3 w[t\text{-}\tau(s_1)]\right\}\gamma(s_1)ds_1 ds \\ &+ \int_{-s_a}^{s_s}\cos\beta(s)\int_{-s_0}^{-s_a}\int_{-s_0}^{s_1}\left\{\alpha_2\ddot{w}[t\text{-}\tau(s_2)]+\alpha_4\dot{w}[t\text{-}\tau(s_2)]\right\}\gamma(s_2)ds_2 ds_1 ds \\ &+ \int_{-s_a}^{s_s}\cos\beta(s)\int_{-s_a}^{s}\int_{-s_0}^{-s_a}\left\{\alpha_2\ddot{w}[t\text{-}\tau(s_2)]+\alpha_4\dot{w}[t\text{-}\tau(s_2)]\right\}\gamma(s_2)ds_2 ds_1 ds \end{aligned} \tag{B.10}$$

References

[1] M. Païdoussis, A review of flow-induced vibrations in reactor and reactor components, Nucl. Eng. Des. 74 (1982) 31–60.
[2] R. Blevins, Flow-induced vibration in nuclear reactors: a review, Prog. Nucl. Energy 4 (1) (1979) 25–49.
[3] M. Païdoussis, Fluidelastic vibration of cylinder arrays in axial and cross flow: state of the art, J. Sound Vib. 76 (3) (1981) 329–360.
[4] M. Pettigrew, C. Taylor, N. Fisher, M. Yetisir, B. Smith, Flow-induced vibration: recent findings and open questions, Nucl. Eng. Des. 185 (2–3) (1998) 249–276.
[5] M. Pettigrew, C. Taylor, Two-phase flow-induced vibration: an overview, J. Press. Vessel Technol. 116 (3) (1994) 233–253.
[6] D. Weaver, J. Fitzpatrick, A review of cross-flow induced vibrations in heat exchanger tube arrays, J. Fluids Struct. 2 (1) (1988) 73–93.
[7] S. Price, A review of theoretical models for fluidelastic instability of cylinder arrays in cross-flow, J. Fluids Struct. 9 (5) (1995) 463–518.
[8] S. Chen, Flow-Induced Vibration of Circular Cylindrical Structures, Hemisphere, 1987.
[9] M.P. Païdoussis, S.J. Price, E. De Langre, Fluid-Structure Interactions: Cross-Flow-Induced Instabilities, Cambridge University Press, 2010.
[10] M.P. Païdoussis, Fluid-Structure Interactions: Slender Structures and Axial Flow, vol. 1, Academic Press, 1998.
[11] M. Au-Yang, Flow Induced Vibration of Power and Process Plant Components: A Practical Workbook, Flow Induced Vibration of Power and Process Plant Components: A Practical Workbook, 2001.
[12] M.J. Pettigrew, C.E. Taylor, N.J. Fisher, Flow-Induced Vibration Handbook for Nuclear and Process Equipment, John Wiley & Sons, 2021.
[13] T. Nakamura, S. Kaneko, F. Inada, M. Kato, K. Ishihara, T. Nishihara, N.W. Mureithi, M.A. Langthjem, Flow-Induced Vibrations: Classifications and Lessons from Practical Experiences, Butterworth-Heinemann, 2013.
[14] B.W. Roberts, Low frequency, aeroelastic vibrations in a cascade of circular cylinders, in: Mechanical Science Monograph (4), 1966.
[15] H. Conners, Fluidelastic vibration of tube arrays excited by cross flow, in: Proc. ASME Winter Annual Meet, 1970, pp. 42–56.
[16] H. Connors, Fluidelastic Vibration of Heat Exchanger Tube Arrays, 1978.
[17] R. Blevins, Fluid elastic whirling of a tube row, Trans. ASME, J. Press. Vessels Tech. (1974) 263–267.
[18] V. Shinde, E. Longatte, F. Baj, M. Braza, A theoretical model of fluidelastic instability in tube arrays, Nucl. Eng. Des. 337 (2018) 406–418.
[19] H. Tanaka, S. Takahara, Unsteady fluid dynamic force on tube bundle and its dynamic effect on vibration, in: ASME Century 2 Emerging Technology Conference, 1980.
[20] H. Tanaka, S. Takahara, Fluid elastic vibration of tube array in cross flow, J. Sound Vib. 77 (1) (1981) 19–37.
[21] S. Chen, Instability mechanisms and stability criteria of a group of circular cylinders subjected to cross-flow, Part I: Theory, ASME J. Vib. Acoust. Stress Reliab. Des. 105 (1983) 51–58.
[22] S. Chen, Instability mechanisms and stability criteria of a groupe of circular cylinders subjected to cross flow; Part 1: Theory, Part 2: Numerical results and discussions, J. Vib. Acoust. Stress Reliab. Des. 105 (1983) 253–260.
[23] S. Chen, A general theory for dynamic instability of tube arrays in crossflow, J. Fluids Struct. 1 (1987) 35–53.
[24] S. Price, M. Païdoussis, A theoretical investigation of the parameters affecting the fluidelastic instability of a double row of cylinders subject to cross-flow, in: Proceedings 3rd International Conference on Vibrations in Nuclear Plant, 1982, pp. 107–119.
[25] S. Price, M. Païdoussis, Fluidelastic instability of a double row of circular cylinders subject to cross-flow, ASME J. Vib. Acoust. Stress Reliab. Des. 105 (1983) 59–66.
[26] J. Lever, D. Weaver, A theoretical model for fluid-elastic instability in heat exchanger tube bundles, ASME J. Press. Vessel Technol. 104 (1982) 147–158.
[27] J. Lever, D. Weaver, On the stability of heat exchanger tube bundles, Part I: Modified theoretical model, J. Sound Vib. 107 (3) (1986) 375–392.
[28] J. Lever, D. Weaver, On the stability of heat exchanger tube bundles. Part II. Numerical results and comparison with experiments, J. Sound Vib. 107 (3) (1986) 375–410.
[29] M. Yetisir, D. Weaver, On an unsteady theory for fluidelastic instability of heat exchanger tube arrays, in: 1988 International Symposium on Flow-Induced Vibrations and Noise, vol. 3, 1988, pp. 181–195.

[30] M. Yetisir, D. Weaver, Theoretical Study of Fluidelastic Instability in a Flexible Array of Tubes, vol. 242, ASME, New York, NY(USA), 1992, pp. 69–87.
[31] M. Yetisir, D. Weaver, An unsteady theory for fluidelastic instability in an array of flexible tubes in cross-flow. Part I: Theory, J. Fluids Struct. 7 (7) (1993) 751–766.
[32] M. Yetisir, D. Weaver, An unsteady theory for fluidelastic instability in an array of flexible tubes in cross-flow. Part II: Results and comparison with experiments, J. Fluids Struct. 7 (7) (1993) 767–782.
[33] A. Fricker, Numerical analysis of the fluidelastic vibration of a steam generator tube with loose supports, in: J.M. Chenoweth, S.S. Chen, J.R. Stenner, W.J. Bryan (Eds.), Proceedings ASME International Symposiam on Flow-Induced Vibration and Noise, vol. 5: Flow-Induced Vibration in Heat-Transfer Equipment, 1988, pp. 105–120.
[34] A. Fricker, Numerical analysis of the fluidelastic vibration of a steam generator tube with loose supports, J. Fluids Struct. 6 (1) (1992) 85–107.
[35] F. Eisinger, M. Rao, D. Steininger, K. Haslinger, Numerical simulation of cross-flow-induced fluidelastic vibration of tube arrays and comparison with experimental results, J. Press. Vessel Technol. 117 (1) (1995) 31–39.
[36] T. Sawadogo, N. Mureithi, Simulation of the vibration of a steam generator tube subjected to fluidelastic forces induced by two-phase cross-flow, in: Pressure Vessels and Piping Conference, vol. 44540, 2011, pp. 151–162.
[37] T. Sawadogo, N. Mureithi, Time domain simulation of the vibration of a steam generator tube subjected to fluidelastic forces induced by two-phase cross-flow, J. Press. Vessel Technol. 135 (3) (2013).
[38] P. Piteau, X. Delaune, J. Antunes, L. Borsoi, Experiments and computations of a loosely supported tube in a rigid bundle subjected to single-phase flow, J. Fluids Struct. 28 (2012) 56–71.
[39] M. Païdoussis, G. Li, Cross-flow-induced chaotic motions of heat-exchanger tubes impacting on loose supports, in: Flow-Induced Vibrations and Wear, ASME, New York, 1991, pp. 31–41.
[40] N. Mureithi, S. Price, M. Paidoussis, The post-Hopf-bifurcation response of a loosely supported cylinder in an array subjected to cross-flow. Part I: Experimental results, J. Fluids Struct. 8 (7) (1994) 833–852.
[41] N. Mureithi, M. Paidoussis, S. Price, The post-Hopf-bifurcation response of a loosely supported cylinder in an array subjected to cross-flow. Part II: Theoretical model and comparison with experiments, J. Fluids Struct. 8 (7) (1994) 853–876.
[42] P. Sun, X. Zhao, X. Yu, Q. Huang, Z. Feng, J. Zhou, Incremental harmonic balance method for multi-harmonic solution of high-dimensional delay differential equations: application to crossflow-induced nonlinear vibration of steam generator tubes, Appl. Math. Model. 118 (2023) 818–831.
[43] M. Hassan, M. Hayder, Modelling of fluidelastic vibrations of heat exchanger tubes with loose supports, Nucl. Eng. Des. 238 (10) (2008) 2507–2520.
[44] M. Hassan, A. Hossen, Time domain models for damping-controlled fluidelastic instability forces in tubes with loose supports, J. Press. Vessel Technol. 132 (4) (2010).
[45] M.A. Hassan, R.J. Rogers, A.G. Gerber, Damping-controlled fluidelastic instability forces in multi-span tubes with loose supports, Nucl. Eng. Des. 241 (8) (2011) 2666–2673.
[46] M. Hassan, A. Mohany, Fluidelastic instability modeling of loosely supported multispan u-tubes in nuclear steam generators, J. Press. Vessel Technol. 135 (1) (2013).
[47] M. Hassan, D.S. Weaver, Modeling of streamwise and transverse fluidelastic instability in tube arrays, J. Press. Vessel Technol. 138 (5) (2016).
[48] B. Anderson, M. Hassan, A. Mohany, Modelling of fluidelastic instability in a square inline tube array including the boundary layer effect, J. Fluids Struct. 48 (2014) 362–375.
[49] S.H. Chen, S.S. Chen, Chaotic vibration in fluidelastic instability of a tube row in crossflow, Tech. Rep., Argonne National Lab., IL (United States), 1993.
[50] S.S. Chen, S. Zhu, Y. Cai, Experiment on fluidelastic instability of loosely supported tube arrays in crossflow, Tech. Rep, Argonne National Lab., IL (United States), 1993.
[51] Y. Cai, S.S. Chen, Chaotic dynamics of loosely supported tubes in crossflow, Tech. Rep., Argonne National Lab., IL (United States), 1991.
[52] M.P. Païdoussis, G.X. Li, Cross-flow-induced chaotic vibrations of heat-exchanger tubes impacting on loose supports, J. Sound Vib. 152 (2) (1992) 305–326.
[53] J. Lai, L. Sun, P. Li, Two-phase flow-induced instability and nonlinear dynamics of a single tube in tube bundles in the transverse direction, Eur. J. Mech. A, Solids 78 (2019) 103858.
[54] V. Shinde, E. Longatte, F. Baj, Large eddy simulation of fluid-elastic instability in square normal cylinder array, J. Press. Vessel Technol. 140 (4) (2018) 041301.
[55] O.L. Pierson, Experimental investigation of the influence of tube arrangement on convection heat transfer and flow resistance in cross flow of gases over tube banks, Trans. Am. Soc. Mech. Eng. 59 (7) (1937) 563–572.
[56] D. Weaver, J. Parrondo, Fluidelastic instability in multispan heat exchanger tube arrays, J. Fluids Struct. 5 (3) (1991) 323–338.
[57] H. Tanaka, S. Takahara, K. Ohta, Flow-induced vibration of tube arrays with various pitch-to-diameter ratios, J. Press. Vessel Technol., Trans. ASME 104 (3) (1982) 168–174.
[58] M. Païdoussis, S. Price, D. Mavriplis, A semipotential flow theory for the dynamics of cylinder arrays in cross flow, J. Fluids Eng. 107 (4) (1985) 500–506.
[59] C. Teh, H. Goyder, M. Païdoussis, S. Chen, M. Bernstein, Data for the fluidelastic instability of heat exchanger tube bundles, in: Proceedings of the International Conference on Flow Induced Vibration Noise: Flow-Induced Vibration and Noise in Cylinder Arrays, Chicago, IL, 1988, pp. 77–94.
[60] J. Lever, G. Rzentkowski, Dependence of post-stable fluidelastic behavior on the degrees of freedom of a tube bundle, J. Fluids Struct. 7 (5) (1993) 471–496.
[61] T. Nakamura, K. Fujita, A. Tsuge, Two-phase cross-flow-induced vibration of tube arrays: brief review of previous studies and summary of design methods, JSME Int. J. Ser. B Fluids Therm. Eng. 36 (3) (1993) 429–438.
[62] I. Gholami, M. Amabili, M.P. Païdoussis, Dynamic divergence of circular cylindrical shells conveying airflow, Mech. Syst. Signal Process. 166 (2022) 108496.
[63] M. Païdoussis, R. Botez, Three routes to chaos for a three-degree-of-freedom articulated cylinder system subjected to annular flow and impacting on the outer pipe, Nonlinear Dyn. 7 (1995) 429–450.
[64] M. Benaouicha, F. Baj, E. Longatte, An algebraic expansion of the potential theory for predicting dynamic stability limit of in-line cylinder arrangement under single-phase fluid cross-flow, J. Fluids Struct. 72 (2017) 80–95.
[65] L. Alyaldin, N.W. Mureithi, An analytical frequency response function for fluidelastic instability model of a normal triangular array in cross-flow, J. Sound Vib. 561 (2023) 117752.